Hygroscopicity of urban aerosols and its link to size-resolved chemical composition during spring/summertime in Seoul, Korea

Najin Kim[1], Seong Soo Yum[1*], Minsu Park[1], Jong Sung Park[2], Hye Jung Shin[2], Joon Young Ahn[2]

[1]Department of Atmosphere Science, Yonsei university, Seoul, 03722, Korea

[2]Air Quality Research Division, National Institute of Environment Research, Incheon, 22689, Korea

Correspondence to: Seong Soo Yum (ssyum@yonsei.ac.kr)

Abstract. Chemical effects on the size-resolved hygroscopicity of urban aerosols were examined based on the KORUS-AQ field campaign data. The information on size-resolved hygroscopicity and chemical composition of aerosols were obtained by a hygroscopic tandem differential mobility analyzer (HTDMA) and a high-resolution time of flight aerosol mass spectrometer (HR-ToF-AMS), respectively. Good correspondence was shown between measured and estimated κ values calculated from the combination of bulk chemical composition data and oxidation parameters of organic aerosols (f_{44} and O/C). These results imply that chemical composition is closely associated with aerosol hygroscopicity. However, the correlation between measured and estimated κ values degraded as particle size decreased, implying that size-resolved chemical composition data is required for more detailed hygroscopicity analysis. In addition to size-resolved chemical data, the m/z tracer method was applied for size-resolved organic factors. Specifically, m/z 57 and 44 were used as AMS spectral markers for HOA and OOA, respectively. These size-resolved chemical composition data were found to be critical in explaining size-dependent hygroscopicity as well as the diurnal variation of κ for small particles, i.e., low κ in the morning and high κ in the afternoon. Additionally, aerosol mixing state information was associated with the size-resolved chemical composition data. That is, the relationship between the number fraction of each hygroscopicity mode and volume fraction of different chemical composition was investigated. For example, the HOA volume fraction explained about 60 % of the variation of less hygroscopic (LH) mode number fraction for externally mixed aerosols.

    1. Introduction

Aerosol hygroscopicity, an ability of aerosols to absorb water vapor, describes an interaction between water vapor and particles under sub- and supersaturated conditions and determines the critical supersaturation for cloud droplet activation (McFiggans et al., 2006; Swietlicki et al., 2008). In general, aerosols can be characterized as hygroscopic, neutral or hydrophobic, depending on their affinity for water (Rogers and Yau; 1989). Hygroscopicity of aerosols is considered a crucial parameter in aerosol studies as it affects the number concentration of cloud condensation nuclei (CCN) and the lifetime of clouds, and thereby indirectly influences regional and global climate change (Zhang et al., 2008; Su et al., 2010; IPCC, 2013; Rosenfeld et al., 2014). Moreover, hygroscopicity is responsible for degradation of visibility and multiphase chemical reactions, which are closely related to air quality as cross-sectional areas of aerosol particles increase after particles take up water vapor with humidity (Tang et al., 1996; Cheng et al., 2008; Liu et al., 2013; Zheng et al., 2015).

Hygroscopicity measurement has been mainly performed with a hygroscopic tandem differential mobility analyzer (HTDMA) introduced by Liu et al., (1978), and/or with a combined system of a CCN counter (CCNC), a differential mobility analyzer (DMA) and a condensation particle counter (CPC) (Moore et al., 2010; Kim et al., 2011). Particularly, HTDMA provides information of the hygroscopic growth factor (GF) distribution at a given dry particle diameter for a fixed relative humidity (RH). Furthermore, we can infer the extent of the mixing state of aerosols, i.e., external versus internal mixing, through HTDMA measurements (Swietlicki et al. 2008). If internally mixed, all particles are considered to have identical composition and hygroscopicity, whereas external mixing indicates that particles of different composition and hygroscopicity coexist in a sample volume. So, even if the sizes of particles are the same, the critical supersaturation for activation could vary, depending on the mixing state of atmospheric particles. From HTDMA measurements, we may obtain a monomodal GF distribution for perfect internal mixtures, or bimodal or trimodal GF distribution (sometimes more than trimodal) for external mixture of atmospheric aerosols. Various field experiments around the world have conducted

hygroscopicity measurements for ambient aerosols. In marine environments, including Pacific, Indian and Arctic Oceans, atmospheric particles had higher GF than in other environments and mostly showed a monomodal pattern of GF distribution (Berg et al., 1998; Massling et al., 2003, 2006; Swietlicki et al., 2000; Tomlinson et al., 2007; Zhou et al., 2001). In rural sites, both aged and freshly formed particles were observed, and mixing state patterns tended to be different depending on location. Aerosols in the pristine Amazon forest showed moderate GF values due to organic compounds (Rissler et al., 2004; Thalman et al., 2017; Zhou et al., 2002). Hygroscopic properties of aerosols in urban regions where considerable anthropogenic emissions exist have been measured actively in recent years (Baltensperger et al., 2002; Cocker et al., 2001; Massling et al., 2005; Wang et al., 2017; Wu et al., 2016). The external mixture of hygroscopic aerosols from the background and freshly emitted hydrophobic aerosols was dominantly observed in these regions.

In addition to direct measurements, various estimation methods to derive aerosol hygroscopicity have been suggested based on the relationship between chemical composition and hygroscopicity (Chang et al., 2010; Gunthe et al., 2009; Gysel et al., 2007; Wu et al., 2013). In general, the Zdanovskii-Stokes-Robinson (ZSR) mixing rule (Zandnovskii, 1948; Stokes and Ronbinson, 1966) was applied for the estimates. Inorganic aerosols are well known to be hygroscopic from many field and laboratory studies. However, the hygroscopicity of organic materials that occupied a significant portion of atmospheric aerosols (Zhang et al., 2007) is relatively unknown and shows various water uptake abilities. Recent studies have focused on examining the hygroscopic properties of organics based on the measurements of organic fraction in various environments (Chang et al., 2010; Wu et al., 2013; Mei et al., 2013; Hong et al., 2015, 2018). According to several previous studies, the oxidation level of organics is the main factor that affects the water uptake ability of the organic fraction in aerosols. Despite these efforts, knowledge on aerosol hygroscopicity is still limited and subject to significant uncertainties due to difficulties in the identification and quantification of numerous organic compounds in ambient aerosols and their hygroscopic properties. Notably, various emission sources and complex

75 chemical mechanisms of aerosol production and the aging processes in urban areas make it difficult to fully understand the hygroscopic properties of aerosols and their link to aerosol chemical composition.

The Seoul Metropolitan Area (SMA) is one of the largest metropolitan areas in the world where commercial, residential, and industrial facilities of Korea are concentrated on a massive scale. The air masses in SMA are influenced not only by local anthropogenic emission sources but also by

80 biogenic sources to the east (Kim et al., 2010) and industrial emissions to the west of SMA (Kim et al., 2018b). Furthermore, long-range transport of air pollutants from the Asian continent significantly impacts SMA air quality. In addition to local and regional sources, atmospheric processes and meteorological conditions affect aerosol properties. Nevertheless, knowledge of aerosol properties and their impact on air quality in SMA is still limited. Therefore, understanding the various sources and

85 complex mechanisms of atmospheric aerosols in SMA is critical in establishing appropriate and effective environmental policies to mitigate air quality problems. Moreover, enhanced understanding of these characteristics of urban aerosols based on reliable measurement data can eventually be utilized for improving the estimation of global climate change.

The Korea-US Air Quality Study (KORUS-AQ) is an international cooperative air quality field

90 study that was conducted over Korea during spring/summer in 2016. A comprehensive set of measurements from aircraft, ships, satellite and ground sites along with air quality model calculations were made to assemble integrated observational data and examine the factors controlling the air quality in East Asia, where air pollution has increased so much in the past decades due to fast industrialization and urbanization (Swietlicki et al., 2008; Larkin et al., 2016). As part of the KORUS-AQ campaign,

95 ground measurements of aerosol properties, gas-phase concentration, and meteorological parameters in SMA were conducted at Olympic Park, a supersite of the campaign.

In this study, we focus on the measurement of size-resolved hygroscopicity and size-resolved chemical composition by a hygroscopic tandem differential mobility analyzer (HTDMA) and a high resolution time of flight aerosol mass spectrometer (HR-ToF-AMS), respectively. Our study aims to

identify the relationship between chemical composition and the hygroscopicity of aerosols in SMA. For this effort, aerosol hygroscopicity is analyzed in association not only with the size-resolved chemical composition data but also with the size-resolved organic factor data. In addition, aerosol hygroscopicity and CCN capability are examined in relation to the mixing state of aerosols.

2. Experimental description

2.1 Measurement site

The KORUS-AQ field campaign was conducted at multiple ground sites as well as in the air above the Korean Peninsula by aircraft (DC-8 and King Air) from May to June 2016. This study focuses only on the ground measurements at Olympic Park, the main supersite of KORUS-AQ, in SMA (37.6ºN, 127.04ºE). The measurement period was 9 May − 15 June. Although the measurement shelter was surrounded by trees and grass fields of the park, this site was mainly influenced by anthropogenic sources from nearby residential areas, and heavy road traffic. A detailed description of the site and the meteorological conditions during the campaign can be found in Kim et al. (2018a). Briefly, Olympic Park, in general, was affected by dominant westerly winds. However, in some periods during the campaign, this pattern disappeared. Specifically, a persistent high pressure with stagnant conditions prevailed on 17-21 May (Period A in Fig.1), and pollution transport from southwestern China occurred on 25-28 May (Period B in Fig.1). As for meteorological conditions, campaign averaged value for relative humidity (RH) and temperature (T) were 61.0 % and 20.8 °C, respectively. Both RH and T in May are generally lower than those in June. The instruments installed in the measurement shelter are described in the following section.
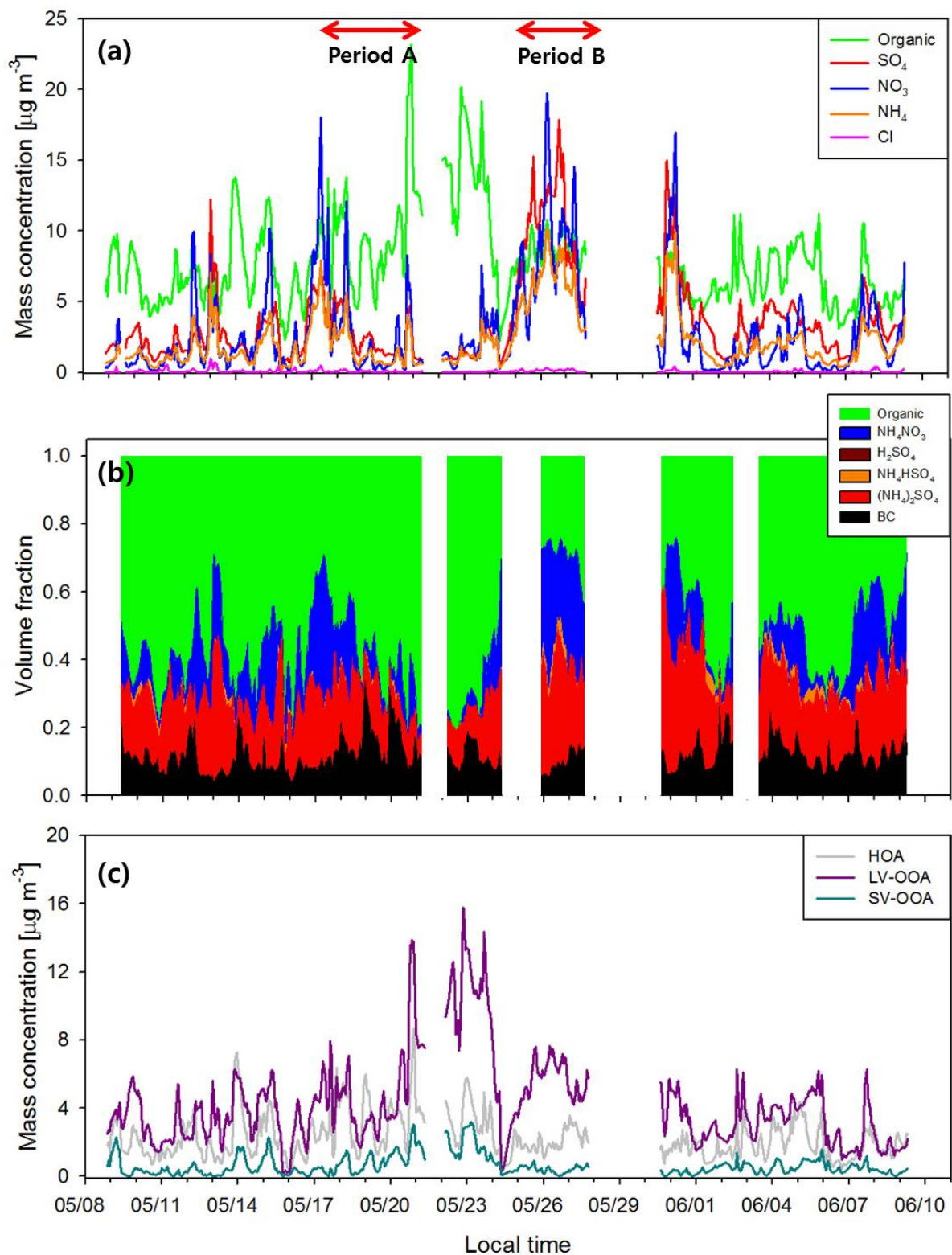
Figure 1. Time series of (a) mass concentration and **(b)** volume fraction of aerosol chemical composition, and **(c)** mass concentration of three organic aerosol (OA) factors (*Additional blank of time series of volume fraction of chemical composition in (b) is due to BC data.)

125

2.2 H-TDMA measurement

The measurement of size-resolved hygroscopicity by HTDMA in Seoul is detailed in Kim et al. (2017, 2018a) and therefore briefly described here. First, ambient aerosols were dried to below 20% RH by silica gel. Next dry aerosols were neutralized by Kr-85 aerosol neutralizer and then were classified to produce monodisperse particles by the first DMA. These classified particles grew under the humid condition of 85% RH. The number size distribution of grown particles was measured by the second DMA with TSI CPC 3010. Two RH sensors were placed at the exit of the Nafion humidifier and sheath air of the second DMA. After the campaign, we conducted the deliquescence relative humidity (DRH) measurement for NaCl and $(NH_4)_2SO_4$ to validate the HTDMA measurement. In this study, four different dry diameters of 30, 50, 100, and 150 nm were chosen to classify in the first DMA for hygroscopicity analysis. The hygroscopic GF, the ratio of humidified (d_w) and dry (d_d) particle mode diameters at a given RH, can be derived from HTDMA output (Eq. 1):

$$GF = \frac{d_w}{d_d} \ .$$
(1)

In this study, we obtained the GF distribution for each dry diameter with 3 min time resolution. The experiment repeated five times for each size. Simultaneously, the information of the mixing state is estimated from the shape of GF distribution and GF values themselves. Kim et al. (2017) suggested an aerosol type classification based on mixing state and GF values as will be briefly introduced later.

2.3 Aerosol chemical composition

Real-time measurement of size-resolved chemical composition is done with a high-resolution time of flight aerosol mass spectrometer (HR-TOF-AMS, Aerodyne Research Inc, USA). It is based on the highly successful design of the first generation quadrupole-based system, the Q-AMS. However, the ToF-AMS differs from the Q-AMS as the quadrupole mass filter is replaced by a time-of-flight mass

spectrometer. In this study, the non-refractory PM_1 (NR-PM_1), particulate matter with an aerodynamic diameter smaller than 1μm that evaporate rapidly at 600 °C under vacuum conditions, were collected using a PM_1 cyclone (URG-2000-30EN, URG, USA). A Nafion drier (Perma-Pure, Toms River, NJ, USA) was used to dry the sampled ambient air. For calibration purposes, ammonium nitrate and polystyrene latex spheres (PSL) particles were produced by using a constant output atomizer (TSI 3936, TSI Inc., USA) from ammonium nitrate and PSL solution, respectively. Ammonium nitrate particles with 300 nm and PSL particles ranging from 50 to 450 nm were used to calibrate the ionization efficiency (IE) and particle size distribution, using a DMA. Mass spectrum data were saved every 5 min resolution. Collection efficiency of 0.5 was applied to all species. The software SQUIRREL V 1.51H and PIKA V 1.10H were used to analyze the collected data.

For the specification of organics, positive matrix factorization (PMF) analysis was performed using the organic compounds of submicron particles. The PMF analysis of organic matters that account for more than 30 % of ultra-fine particles was used to identify aerosol characteristics, depending on the oxidation state. PMF result could provide information about the aging characteristic of organic matters such as the effect of direct emission or long-distance transport. The PMF Evaluation Tool (PET V 2.06) was used to analyze mass spectrum for mass-to-charge ratios (m/z) from 12 to 100. The modeling conditions are as follows: 1) MDL(method detection limit) = 0.15 μg m^{-3}; 2) Down weighting of low-signal-to-noise ratio (SNR; 0.2 ~ 2) data; 3) no use of bad-SNR (under 0.2) data; 4) Down weighting of repeated information (m/z 44 and related m/z values). Factor analysis was performed according to the PMF analysis procedure described by Zhang et al. (2005) and the pre-processing of input data for each step of PMF followed the method suggested by Ulbrich et al., (2009). Down-weighting is a process by lowering the weight of m/z, which may has higher noise than signal, and thereby lower the error and Q-value (Paatero and Hopke 2003). In this study, three organic aerosol (OA) factors are used: 1) hydrocarbon-like organic aerosol (HOA), 2) semi-volatile oxygenated organic aerosol (SV-OOA), and 3) low-volatility oxygenated organic aerosol (LV-OOA). Figure S1 shows the high resolution mass spectra

and time series of the three OA factors.

Mass concentration of black carbon (BC) was measured by the multi-angle absorption photometer (MAAP) with a $PM_{2.5}$ inlet system as HR-TOF-AMS only provides information on chemical composition for non-refractory (NR) aerosols. In this study, other refractory and semi-refractory aerosols like mineral dust and sea salt aerosols that have their own hygroscopic properties were not considered as they were likely to account for little portion of submicron aerosols. For example, sea salt aerosol occupied less than 3% among $PM_{2.5}$ aerosols from a 24 hour period air sample collected in Seoul (Heo et al., 2009). The very good κ-closure results in Fig. 3, which did not consider mineral dust and sea salt, perhaps infer that mineral dust and sea salt aerosols had little effect on the κ-closure analysis.

3. Overview of hygroscopic and chemical properties of aerosols

3.1 Temporal variation of aerosol chemical composition

Figure 1 shows the temporal variations of aerosol chemical compositions, including sulfate, nitrate, ammonium and, organics, at Olympic Park during the campaign period. The bulk mass concentration of PM_1 (=NR-PM_1+BC) ranged from 4.4 to 57.1 μg m^{-3} with a mean value of 19.1 μg m^{-3} and there was substantial variation of chemical composition (Fig.1a). Among non-refractory aerosols, organics occupied about 42.5 % of total mass concentration of PM_1 aerosols during the whole period followed by sulfate (28.4%), nitrate (16.3%), ammonium (12.2%) and chloride (0.6%). Campaign averaged BC mass concentration was about 2.5 μg m^{-3}. In this study, 1300 kg m^{-3} and 1700 kg m^{-3} were assumed for densities of organic (Cross et al., 2007; Florou et al., 2017) and BC (Wu et al., 2013), respectively, to calculate the volume for each species. For BC, PM 2.5 mass concentration is used for calculation, assuming that BC mass is mainly determined by submicron particles (e.g., Clarke et al., 2004; Wu et al., 2013). It can be said from the good agreement between predicted and measured

NH_4^+ that observed anions (SO_4^{2-}, NO_3^- and Cl^-) are fully neutralized by NH_4^+ (Fig. S2) and ion species mainly existed in the form of $(NH_4)_2SO_4$ and NH_4NO_3 (Reilly and Wood (1969); Gysel et al. (2007)). Predominant volume fractions of $(NH_4)_2SO_4$ and NH_4NO_3 among inorganic compounds can also be found in Fig 1b. For organics, HOA, SV-OOA, and LV-OOA accounted for 32.0%, 8.8%, and 59.2%, respectively, of the total OA mass concentration during the campaign.

Chemical composition of PM₁ aerosol showed substantial variation, especially for periods A and B. Organics were dominant in period A when stagnant conditions prevailed due to persistent high atmospheric pressure and weak synoptic flow (Kim et al. 2018a). The average ratio of organic to (inorganic + BC) was 1.60 ±0.82, ranging from 0.48 to 3.60. The average mass concentrations of each chemical species during period A were 7.9 µg m⁻³ (organic), 3.7 µg m⁻³ (sulfate), 2.9 µg m⁻³ (nitrate), 2.2 µg m⁻³ (ammonium) and 2.4 µg m⁻³ (BC). At the beginning of period A, mass concentrations of both HOA and LV-OOA increased sharply, and that of LV-OOA remained high until 23 May (Fig.1c). For period B, total mass concentration increased as polluted air masses were transported directly from southwestern China, and inorganics were dominantly observed with a mean value of 0.32 for organic/(inorganic + BC). The volume fraction of inorganics reached up to 80% during period B. These contrasting chemical compositions of the two periods result in very different hygroscopic properties of aerosols for these two periods (Kim et al. 2018a). For example, hygroscopicity values of period A, an organic-dominant period, was much lower than the normal period that excludes periods A and B, although particle sizes are larger than those in the normal period.

3.2 Size-resolved hygroscopicity of urban aerosols

As mentioned above, size-resolved hygroscopicity for four dry diameters (30, 50, 100, and 150 nm) was measured during the campaign. The average value of κ, a representative single hygroscopicity parameter (Petters and Kreidenweis 2007), ranged from 0.11 to 0.24 with distinct diurnal variation (Kim

et al., 2018a). Figure 2 shows the size-resolved κ values measured in SMA from the two campaigns (MAPS-Seoul and KORUS-AQ) as well as the results from some other urban measurements including Shanghai (Ye et al., 2013), Beijing (Wang et al., 2018), the Pearl River Delta (PRD) region (Jiang et al., 2016) and Paris (Jurányi et al., 2013). The κ values in the figure were derived from HTDMA GF measurements except for Paris that derived κ from CCN measurement. The κ values of SMA were lower than those in Shanghai and similar to Beijing but the lowest κ values were observed from Paris for most diameters. According to Fig.2, most κ values increase with particle size. It is closely related to the fact that the mass fraction of inorganic species increases with increasing particle size (Fig. S3). Inorganic components measured by AMS are considered as the major water-soluble chemical components, influencing the hygroscopic behavior of atmospheric aerosols. Wu et al. (2016) showed increase of the particle number fraction of hydrophilic mode with increasing particle size, and this trend was more conspicuous for smaller particles (< 150 nm). The size-dependency of κ is also shown in other environments such as coastline in UK (Gysel et al., 2007), forested site in Colorado (Levin et al. 2012, 2014) and Wakayama, Japan (Deng et al., 2019), and boreal environment in Finland (Paramonov et al. 2013). Although the Kelvin effect may cause some decrease of κ with decreasing particle size, this effect is small, less than 5%, for particles in the diameter ranged from 50 to 200 nm (Swietlicki et al., 2008; Wang et al., 2018). The average κ values of urban aerosols shown in Fig. 2 are smaller than 0.3 for diameters smaller than 300 nm, implying that the suggested typical continental κ value of 0.3 by Andreae and Rosenfeld (2008) is an overestimation for these urban aerosols. Consequently, it can cause the over-prediction of CCN number concentration (N_{CCN}) in urban areas.
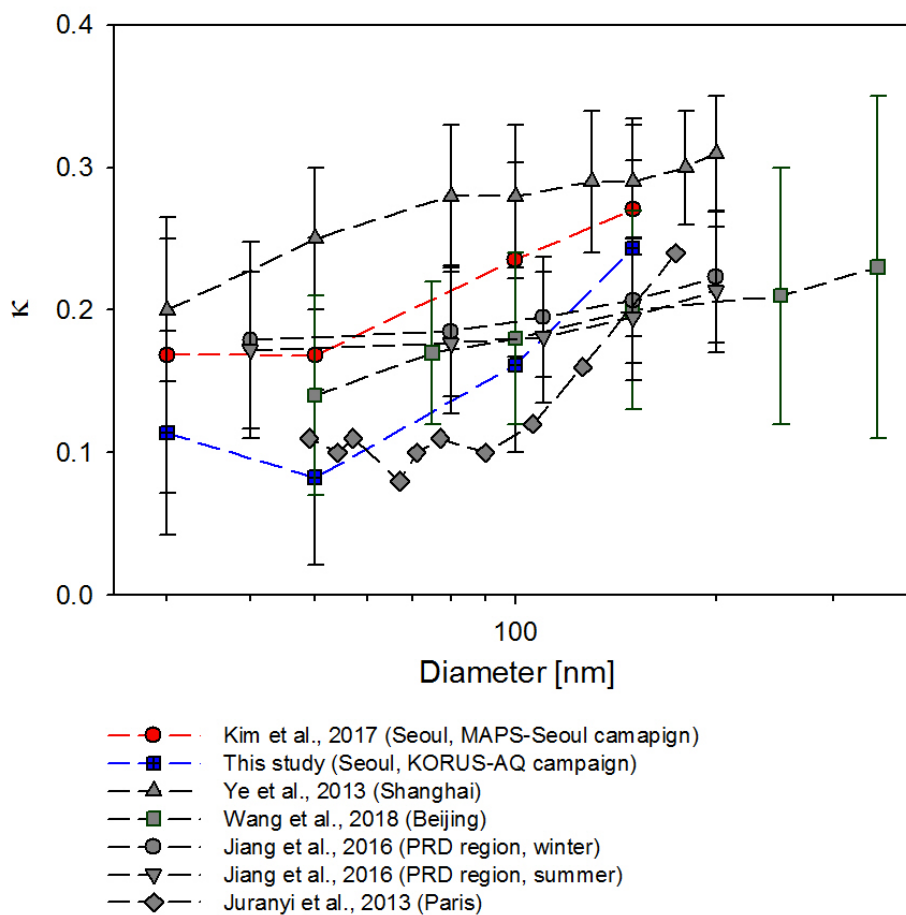
Figure 2. Size-resolved hygroscopicity of aerosols in Seoul and other urban areas.

245

3.3 κ closure

Closure on hygroscopicity has been studied to understand the relationship between chemical composition and aerosol hygroscopicity (Chang et al., 2010; Gunthe et al., 2009; Gysel et al., 2007; Kim et al., 2017; Wu et al., 2013). The ZSR mixing rule (Eq. 2) with a volume fraction of aerosol
250 composition is generally applied for the hygroscopicity closure.

$$\kappa_{chem} = \sum_i \varepsilon_i \kappa_i \, , \qquad (2)$$

where κ_{chem} is the κ value of the mixed particle, κ_i is the hygroscopicity value of the

chemical component, i, in pure form and ε_i is the volume fraction of this chemical component. Unlike inorganic species, the hygroscopicity of organic aerosol (OA) is relatively unknown, and many estimation methods have been suggested for κ-closure. In general, oxidation parameters like O/C and f_{44} are used for the organic hygroscopicity. Among them, we compared the two methods suggested by Kim et al. (2017) that uses O/C (Eq. (3)) and by Mei et al. (2013) (Eq. (4)) that uses f_{44}:

$$\kappa_{org} = 0.1 \times (O/C), \tag{3}$$

$$\kappa_{org} = 2.10(\pm0.07) \times f_{44} - 0.11(\pm0.01). \tag{4}$$

For inorganics, $(NH_4)_2SO_4$ and NH_4NO_3, κ values of 0.47 and 0.58 are applied, respectively (Gysel et al., 2007; Topping et al., 2005). BC is assumed to be hydrophobic.

Figure 3 presents the scatterplot of κ_{HTDMA} vs. κ_{chem}, which incorporates the κ_{org} values derived from the two estimation methods above. Only 150 nm results are used for κ_{HTDMA}. The agreement between κ_{HTDMA} and κ_{chem} looks good regardless of the κ_{org} estimation method and therefore it can be said that such oxidation parameters are suitable to use for estimating hygroscopicity of organic aerosols. Perhaps the similar results of the two methods was in part due to the fact that inorganic species having high κ values compared to organics occupied a major portion of the total mass. In this study, we adopted the method using f_{44} for further analysis because it produced better results than the method using O/C, in terms of the linear regression analysis (i.e., slope and the coefficient of determination) and the average ratio between κ_{HTDMA} and κ_{chem} values (Table S1). According to Fig. 4, however, a good agreement between κ_{HTDMA} and κ_{chem} is shown only for 150 nm. As particle size becomes smaller, widely dispersed scatterplots between κ_{HTDMA} and κ_{chem} are shown. Furthermore, the overestimation of κ_{chem} is clearly shown for small particles. It is because large particles mainly determine the volume fraction in bulk chemical composition data. This result implies that size-resolved chemical composition data should be accompanied when we analyze the relationship between hygroscopicity and chemical composition, especially for small particles.
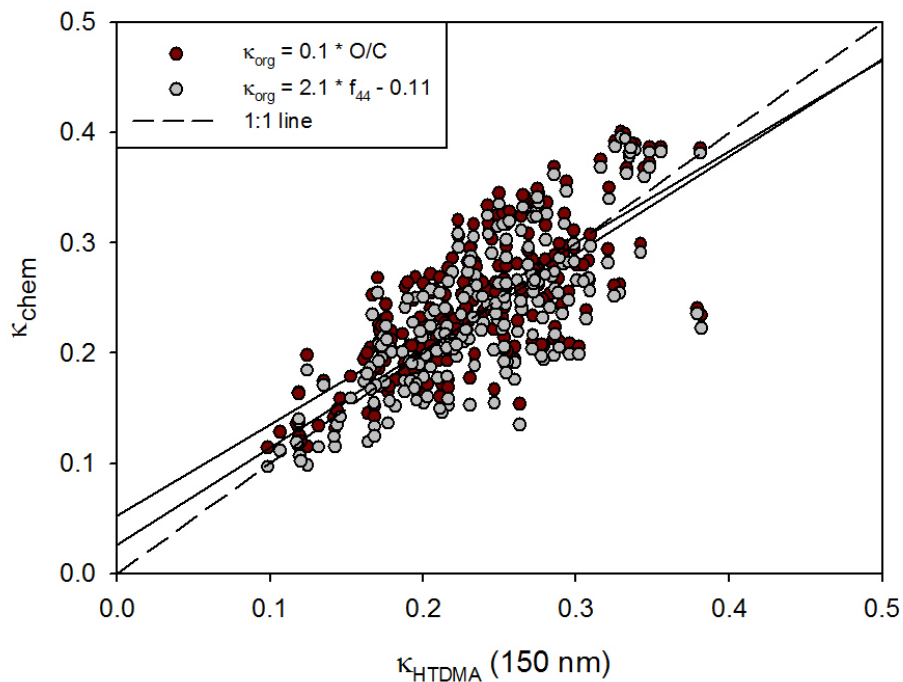
Figure 3. Scatterplot between κ_{HTDMA} and κ_{chem} using two different organic κ estimation methods. Dashed line and solid line indicate 1:1 line and linear regression line, respectively.

280
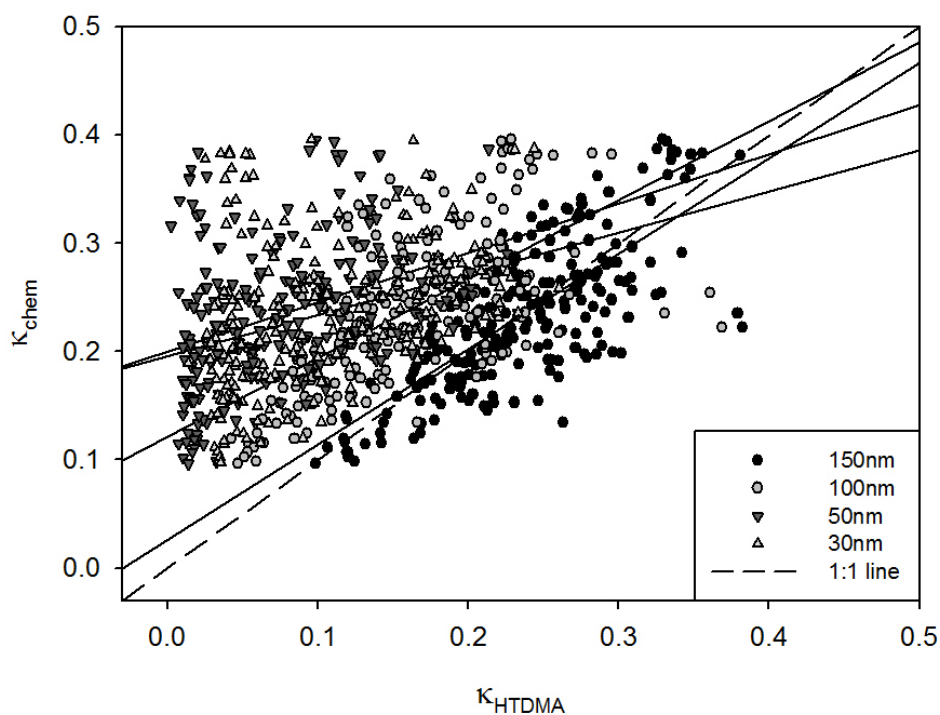
Figure 4. Scatterplot between κ_{HTDMA} and κ_{chem} for four different diameters. Dashed line and solid line indicate 1:1 line and linear regression line, respectively.

4. Size-resolved chemical composition and its link to hygroscopicity and mixing state

285   **4.1 Size-resolved chemical composition**

      The importance of size-resolved chemical composition data has been manifested in the analyses of size-resolved hygroscopicity of aerosols (Bhattu et al., 2016; Levin et al., 2014; Meng et al., 2014). However, particle time-of-flight (P-ToF) mode for the size-resolved species cannot provide sufficient information of mass size distribution directly because of the relatively low signal to noise ratio

290   compared to the bulk mass concentration from mass spectrum (MS) mode. Instead, reconstructed size-resolved mass concentration is applied combining with a bulk mass concentration from the MS mode and a size-resolved mass distribution from the P-ToF mode for individual species as described in Eq. (5) (Thalman et al. 2017).

$$m_i\left(D_p\right) = M_{i,b} \times \frac{\overline{m_i}\left(D_p\right)}{\int_{D_{p,min}}^{D_{p,max}} \overline{m_i}(D'_p)dlogD'_p} \quad , \tag{5}$$

295   where $M_{i,b}$ is the bulk mass concentration from MS mode measurement for chemical species i and $\overline{m_i}(D_p)$ is the average mass size distribution for chemical species i with respect to $logD_p$. $D_{p,max}$ and $D_{p,min}$ indicate the maximum and minimum diameters of the average mass size distribution, respectively. The average mass size distribution for the whole campaign period is shown in Fig. S3; from now on, the reconstructed mass size distribution is denoted as 'size-resolved' for simplicity. It is

300   noted that size-resolved composition data for particles smaller than 70 nm are excluded due to high uncertainties. According to Fig. S3, the mass fraction of organics increases as the particle diameter decreases as expected. Notably, organics occupied more than 70 percent for aerodynamic diameter smaller than 150 nm. In other words, specified organic factor information should be accompanied, especially for small particles, to analyze the size-resolved aerosol hygroscopicity.

305

4.2 Size-resolved organic factors

Zhang et al. (2005) proposed a technique that uses m/z 57 and 44 as AMS mass spectral marker to quantify the mass concentrations of HOA and OOA (= SV-OOA + LV-OOA), using highly time-resolved organic mass spectra obtained with HR-ToF-AMS. m/z 44, most likely CO_2^+, is known to be a major oxygenated organic species in AMS mass spectra and often increases in the afternoon when photochemical reaction is active (Alfarra et a., 2004; Zhang et al., 2005), whereas m/z 57, most likely $C_4H_9^+$, is known to be a major species in mass spectra of hydrocarbon, which is associated with combustion exhaust and often increases in rush hours (Allan et al., 2004 and 2003; Alfarra et al., 2004; Canagaratna et al., 2004). Good correspondences between m/z 57 and HOA and between m/z 44 and OOA for bulk chemical data (not shown) support these assumptions. Although m/z 43 is also known to show a prominent peak for combustion exhaust like m/z 57, it is also influenced by oxygenated organic aerosols ($C_2H_3O^+$) and perhaps that is the reason why the correlation with HOA is not as good as that between HOA and m/z 57 (Fig. S4). Size-resolved organic factors are reconstructed by multiplying a number for each size bin. This number for each reconstructed HOA and OOA is the slope of the linear regression between each organic factor (HOA and OOA) and m/z (57 and 44) from bulk mass concentration. The slopes of the linear regressions are 35.29 and 7.89 for HOA and OOA, respectively. Each reconstructed organic factor is well correlated with the measured one, and the reconstructed organic mass concentration (= HOA + OOA) shows a good correspondence with measured bulk organic mass concentration (Fig. S5). In other words, organic mass concentration in this study can be explained substantially by the two organic factors. Also, m/z 57 and 44 can be considered as first-order tracers of the two major organic components. The correlation coefficient between measured and reconstructed HOA is slightly lower than that of OOA (Fig. S5) because the contribution of m/z 57 on HOA varies depending on time and/or sources, whereas m/z 44 contains a broader range of OOA. Figure 5 shows the campaign averaged size distribution of reconstructed HOA and OOA (From now on, 'reconstructed' HOA and OOA are just called as HOA and OOA in short.). The mode diameter of OOA is somewhat

larger than that of HOA. Mass fraction of HOA is larger than that of OOA for small particles (< 120 nm) but the opposite is true for larger particles (> 120 nm).
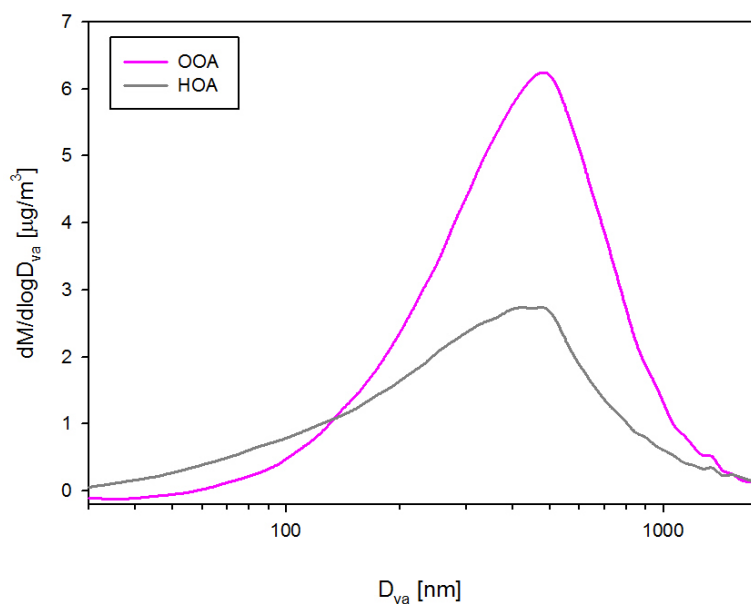
Figure 5. Campaign averaged size distributions of reconstructed HOA (grey) and OOA (pink).

335

4.3 Size-resolved chemical effect on hygroscopicity

Figure 6 presents the campaign averaged size-resolved volume fraction of chemical species with size-resolved κ values. For direct comparison between aerosol hygroscopicity and chemical composition, the conversion of diameter is essential due to different particle sizing techniques (i.e.,

340 mobility diameter (d_m) for HTDMA and vacuum aerodynamic diameter (d_{va}) for AMS). Under the assumption of a spherical particle, d_{va} can be converted into d_m with density information as described in Eq. (6) (DeCarlo et al., 2004).

$$d_m = \frac{\rho_0}{\rho_p} d_{va} \; , \tag{6}$$

where ρ_p is the particle density and ρ_0 is the standard density (1000 kg m^{-3}). In this study,

345 1300 kg m^{-3} is used as the particle density since organics are the most dominant chemical composition

in the particle size range of hygroscopicity measurement. As mentioned above, the κ value of 30 nm particle is excluded due to high uncertainties. Densities of chemical species are assumed for calculation of volume fraction: 930 kg m^{-3} (HOA), 1500 kg m^{-3} (OOA), and 1769 kg m^{-3} (inorganics). For small particles, volume fraction is dominated by organics (= HOA+OOA) and HOA, widely known to be hydrophobic, explains more than 50%. However, the volume fraction of inorganics, which is hygroscopic, increases as particle size increases. Among organics, a sharp decrease of HOA volume fraction and an increase of OOA with size are clearly shown. These results support the size-dependent hygroscopicity. Moreover, the dominant organic volume fraction for small particles (d_{va} < 100 nm) manifests the importance of size-resolved organic factors to explain the variation of hygroscopicity.

Figure 7 illustrates the diurnal variation of κ with chemical composition for 50 nm and 150 nm particles. For 50 nm (Fig. 7a), HOA explained more than 50% among chemical compositions, and the two organic factors showed considerable temporal variation compared to inorganics. The volume fraction of HOA increased slightly in rush hours (07:00-09:00 LT) and decreased gradually after midday until 18:00. Conversely, the volume fraction of OOA decreased in the morning and increased in the afternoon when the photochemical reaction is active. It is consistent with the diurnal variation of κ, showing the relatively low values in the night hours and high values in the late afternoon. On the other hand, for 150 nm (Fig. 7b) chemical compositions showed little variation. Therefore, it can be said that the effect of chemical composition on diurnal variation of κ is more sensitive for small particles than for large particles. Such results demonstrate that, without proper specification of organic factors, it is difficult to explain the diurnal variation of κ. Also noted is that κ variation for small particles is mostly affected by the volume fraction of organics rather than that of inorganics.
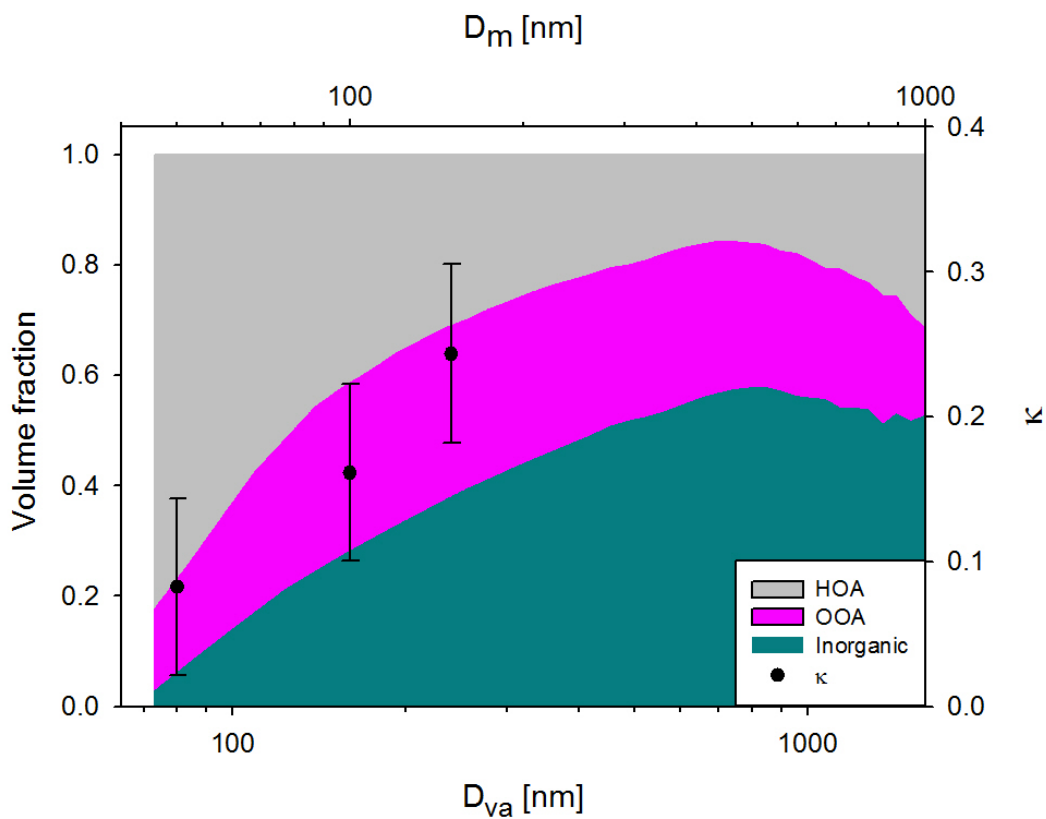
Figure 6. Campaign averaged size-resolved volume fraction of chemical species with κ values (κ_{HTDMA}) for 50, 100 and 150 nm (Mobility diameter (D_m) for κ value is converted to aerodynamic diameter (D_{va}) for comparison).
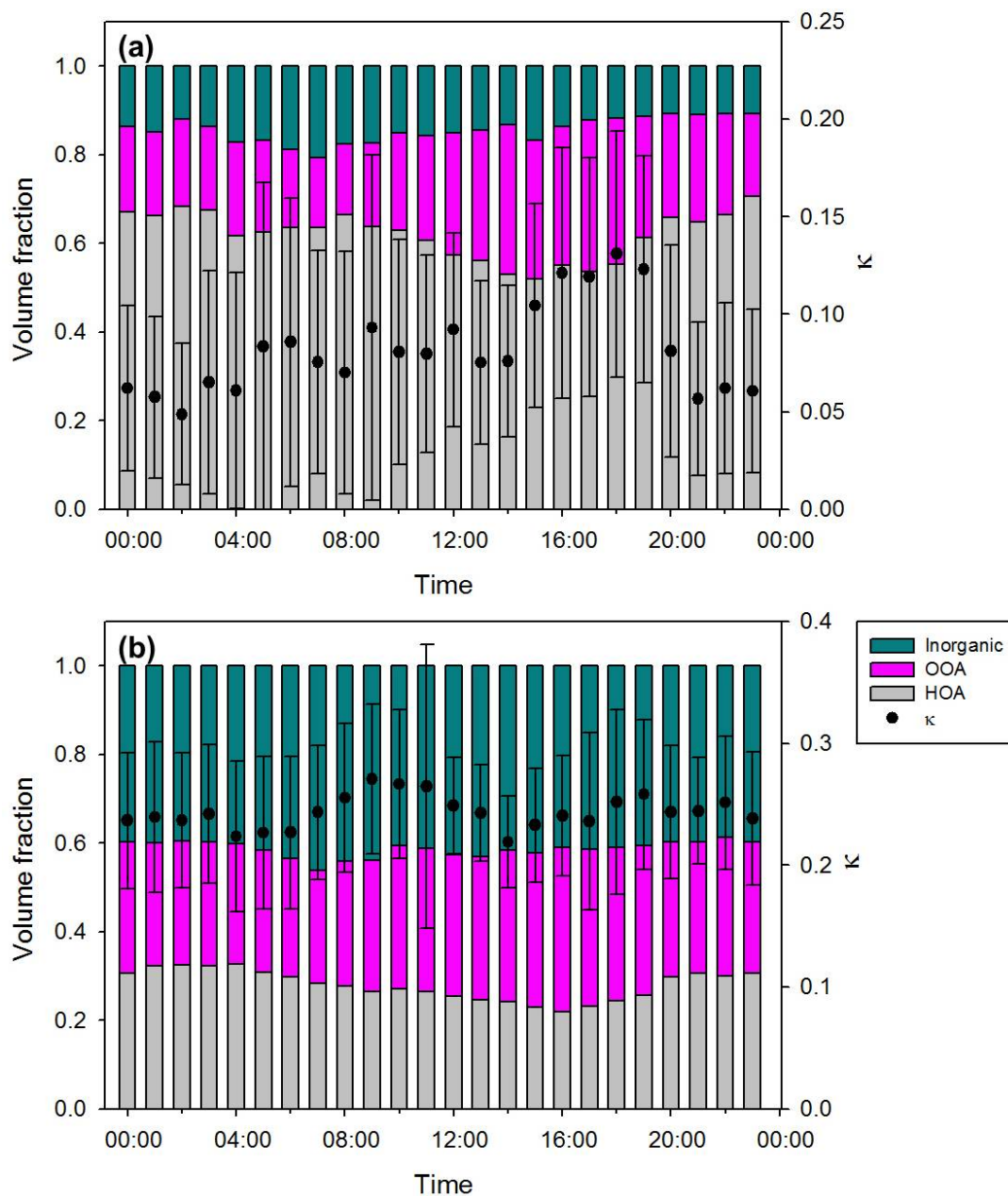
Figure 7. Diurnal variation of κ values (κ_{HTDMA}) and chemical composition of (a) 50 nm and (b) 150 nm particle.

375   As mentioned above, oxidation parameters, such as f_{44} and O/C ratio, are appropriate to use for indicating organic hygroscopicity and thereby several estimation methods using them have been proposed (e.g., Chang et al., 2010; Cerully et al., 2015; Kim et al., 2017; Mei et al., 2013; Hong et al., 2018). Notably, the estimation method using f$_{44}$ (bulk data) produces a good correlation between

measured and estimated κ as shown in Fig. 3. The increase in f_{44} value is known to be the result of

380 photochemical oxidation. The size-dependent κ is also reflected in the degree of oxidation, as can be

seen from the increase in size-resolved f_{44} with increasing particle diameter (Fig.8a). The positive

relationship between size-resolved f_{44} and κ values for 50 nm particles (Fig.8b) also explains that the

oxidation of organics affects the hygroscopic properties of particles. It is noted that data that the volume

fraction of organics is larger than 0.7 were only used to exclude the effect of inorganics. Figure 9

385 presents scatterplots between κ_{org} (30, 50, and 150 nm) and volume fraction of HOA and OOA among

organics. κ_{org} is calculated by subtracting inorganic part from κ_{HTDMA}. As expected, the volume

fraction of HOA was negatively correlated with κ values, whereas that of OOA was positively

correlated with κ values for all sizes of particles. These results demonstrate that the specification of

size-resolved organic factor is an indispensable part of describing the relationship between size-resolved

390 hygroscopicity and chemical composition of aerosols. It is noted that κ_{org} in Fig. 9 is an estimated

value with a simple assumption (see figure caption) to show the relationship between size-resolved

organic factors and hygroscopicity. Negative κ_{org} appears when κ_{inorg} is high even if the volume

fraction of inorganics is low (i.e., low ε_{inorg}).
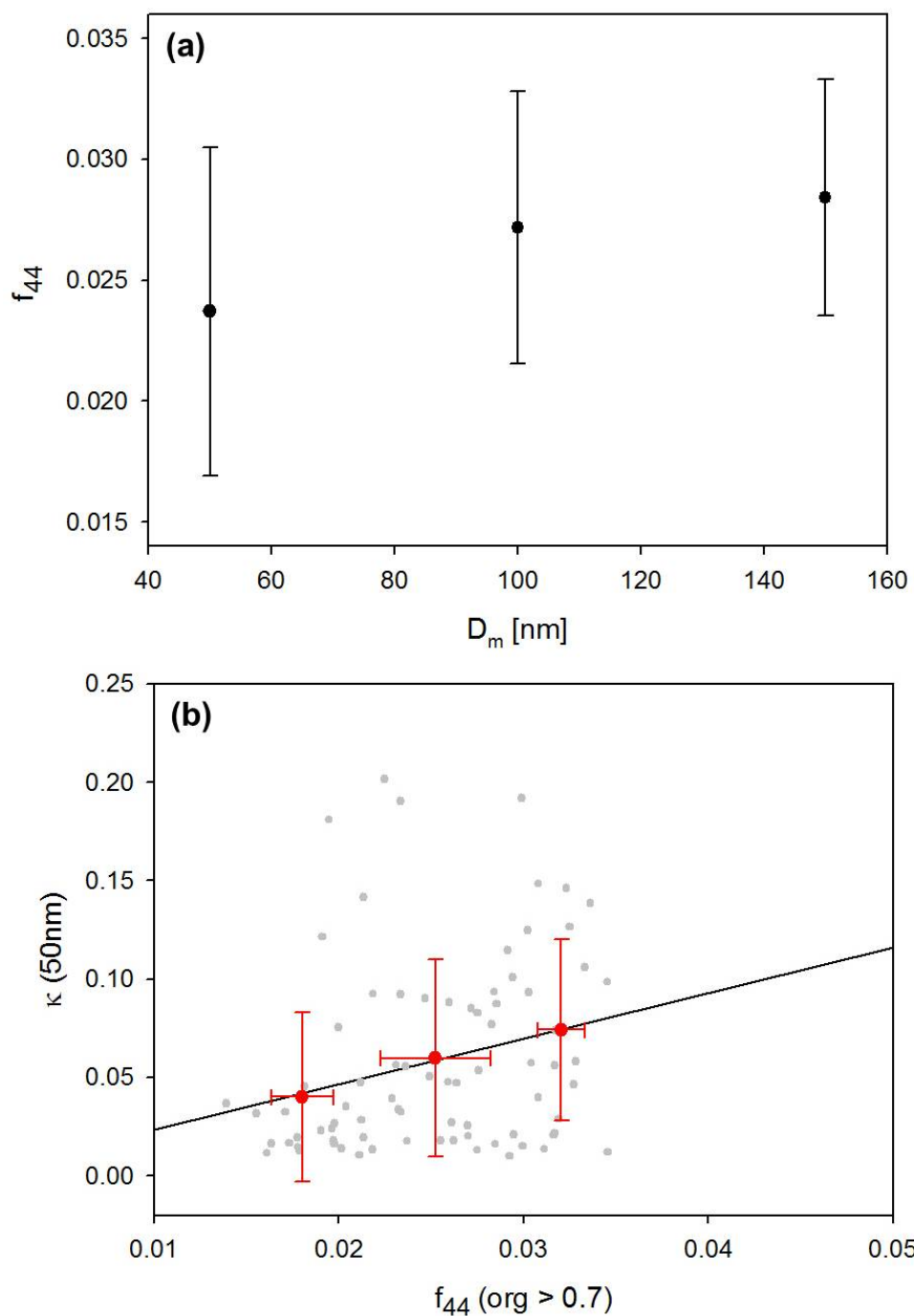
Figure 8. (a) Size-resolved f₄₄ and (b) relationship between f₄₄ and κ values (κ_{HTDMA}) for 50 nm particles (The f_{44} values are only used when organic volume fraction is higher than 0.7). Red dots and bars indicate average and standard deviations for each of the 0.01 interval bins.
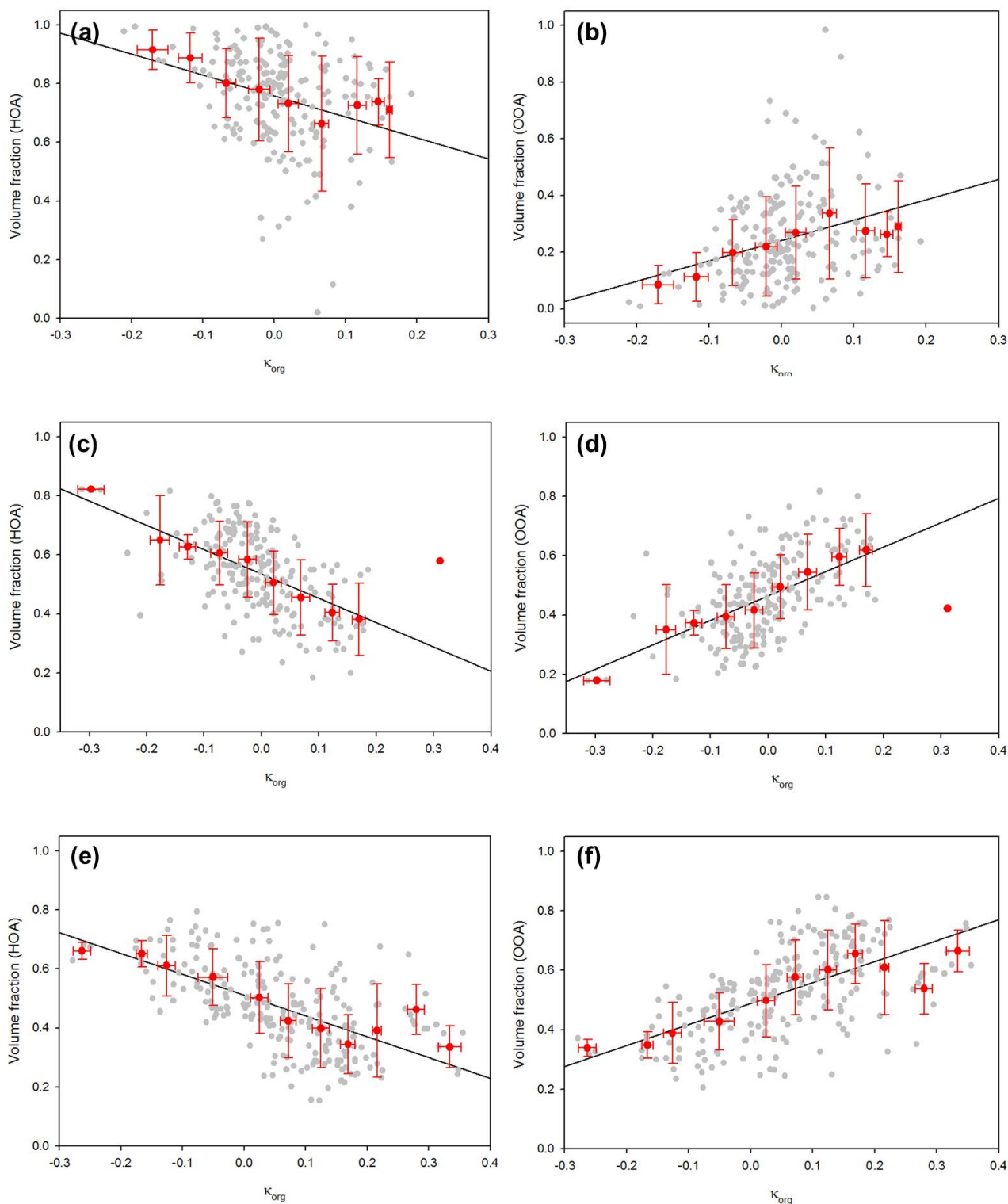
Figure 9 Scatterplot of κ_{org} vs. volume fraction of HOA (left column) and OOA (right column) among organics for 50 nm ((a) and (b)), 100 nm ((c) and (d)) and 150 nm ((e) and (f)) dry diameters. κ_{org} is calculated as: $\kappa_{org} = (\kappa_{HTMDA} - \varepsilon_{inorg}\kappa_{inorg})/\varepsilon_{org}$. ε indicates the volume fraction of each component.

4.4 Relevance to mixing state

HTDMA measurement data can provide information on the mixing state of atmospheric particles, i.e., external or internal mixing. We can also infer the extent of chemical mixing of particles from this information (Swietlicki et al., 2008). External mixing was prevalently observed in Seoul during the MAPS-Seoul (2015), and the KORUS-AQ (2016) campaigns (Kim et al., 2017;2018a) like in other urban regions (Enroth et al., 2018; Wang et al., 2010; Hong et al., 2018). Kim et al. (2017) suggested an aerosol type classification based on the GF values and the mixing state information taken from the HTDMA GF distribution data ($dN/dlog(GF)$); Type 1 (externally mixed aerosols: less and more hygroscopic particles are externally mixed), Type 2 (internally mixed aerosols with GF > 1.1: all particles are more hygroscopic), and Type 3 (internally mixed aerosols with GF < 1.1: all particles are less hygroscopic). Figure 10 presents the schematic plot of three aerosol Types. For determination of mixing state, the position, height and width of each peak for HTDMA data are computed by *peakfit* function for MATLAB® that performs a least-square curve fit of a Gaussian function to the top part of the peak (O'Haver, 2016).
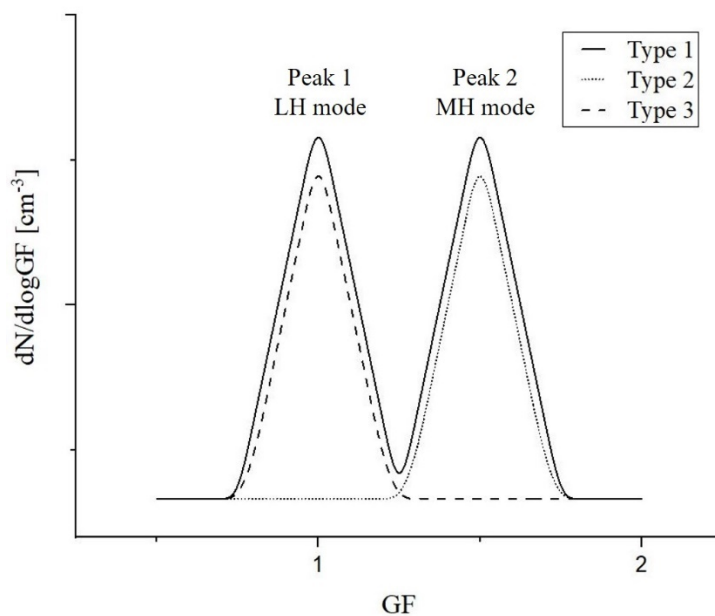
Figure 10. Schematic plot of three aerosol Types: Type 1 (externally mixed aerosol; solid line), Type 2 (internally mixed aerosols with GF > 1.1; dotted line) and Type 3 (internally mixed with GF <1.1;

dashed line).

For externally mixed particles (Type 1), the GF distributions were mostly bimodal but trimodal or higher modal distributions were only occasionally observed (less than 3% of total measurement cases). So, it is safe to assume that externally mixed particles are bimodal. Then the first peak (denoted as Peak 1) in the GF distribution is defined as less hygroscopic (LH) mode that usually had GF value lower than 1.1, and the second peak (denoted as Peak 2) is defined as more hygroscopic (MH) mode that has GF value larger than 1.1. During the measurement period, Type 1 (externally mixed) aerosols were predominantly observed (higher than 70%) in large particles (100 and 150 nm) whereas Type 3 (internally mixed with LH mode) aerosols occupied more than 50% of all aerosols in small particles (30 and 50 nm) (Table S2). Also found was that mixing state had a distinct diurnal pattern, as depicted in Fig. S6. Briefly, for small particles, Type 3 aerosols prevailed all day, except in the afternoon (12:00 – 18:00 LT), when a significant portion of the aerosols turned into Type 2. For large particles, externally mixed aerosols (Type 1) dominated, especially during the rush hour (07:00 – 09:00 LT) when hydrophobic particles emitted from traffics mix with preexisting large and aged particles. In the afternoon, mixing state change occurred in both small and large particles due to the photochemical processes. At night, however, no such change occurred as there was no photochemical process.

Table 1. The area ratio, GF value and κ value for less hygroscopic (LH) mode and more hygroscopic (MH) mode for four dry diameters for all three types of aerosols.

	LH mode area ratio	MH mode area ratio	GF (LH mode)	κ (LH mode)	GF (MH mode)	κ (MH mode)
30 nm	0.61	0.39	1.07	0.05	1.26	0.25
50 nm	0.69	0.31	1.04	0.02	1.28	0.22
100 nm	0.35	0.65	1.01	0.01	1.34	0.25
150 nm	0.22	0.78	1.02	0.01	1.43	0.31

Table 2. The area ratio, GF value and κ value for less hygroscopic (LH) mode and more hygroscopic (MH) mode for four dry diameters for only Type 1 (externally mixed aerosol) aerosol.

	LH mode area ratio	MH mode area ratio	GF (LH mode)	κ (LH mode)	GF (MH mode)	κ (MH mode)
30 nm	0.60	0.40	1.04	0.03	1.34	0.37
50 nm	0.57	0.43	1.01	0.01	1.32	0.25
100 nm	0.42	0.58	1.01	0.01	1.36	0.26
150 nm	0.28	0.72	1.02	0.01	1.45	0.32

445   Table 1 presents the area ratio, GF, and κ value of LH and MH modes for the four different dry diameters. The area ratio of each mode is directly related to the number fraction of each mode as the area is calculated by integrating the GF distribution, $dN/dlog(GF)$, for each mode. The results in Table 1 contain all three types of aerosols. LH mode includes Peak 1 of Type 1 (externally mixed) aerosols and all Type 3 (internally mixed and non-growth) aerosols. MH mode includes Peak 2 of Type

450   1 aerosols and all Type 2 (internally mixed and growth) aerosols. The area ratio of LH mode is substantially high for small particles compared to MH mode, and the area ratio of MH mode becomes larger as particle size increases. It is directly connected to the size-dependency of κ. The GF value of MH mode increases as particle size increases. Table 2 shows only the Type 1 (externally mixed) aerosols for comparison. An increasing trend of MH mode area ratio and GF value with increasing

455   diameter is similar to the results in Table 1. However, GF values of MH mode particles are slightly higher than those in Table 1, especially for smaller diameters (30 nm, 50 nm). It can be explained by the fact that Type 2 (internally mixed and growth) aerosols usually had lower GF values than the MH mode aerosol of Type 1 (externally mixed) aerosols. During the campaign, the number fraction of Type 2 aerosols was the highest in the afternoon, whereas that of Type 3 aerosols was the lowest at that time for

460   all diameters (Kim et al., 2018a). Moreover, a bimodal GF distribution, implying Type 1, in the morning mostly changed to unimodal in the afternoon (Fig.S6). It can be inferred that less hygroscopic particles

gained hygroscopicity due to quick coating by secondary hygroscopic species and LH mode disappeared as the day went on. Kim et al. (2018b) suggested from the strong correlation between OOA vs. O_x that the photochemical reaction occurred actively in the afternoon during the campaign period.

465 Although the GF value of hydrophobic particles increased by coating and GF distribution changed from bimodal to unimodal, the GF values of coated particles (Type 2) were still slightly lower than that of the existing hygroscopic particles, MH mode of Type 1 aerosols.

For N$_{CCN}$ prediction, several studies have considered the mixing state of aerosols with chemical species data (e.g., Bhattu et al., 2015; Ervens et al., 2010; Ren et al., 2018; Wang et al., 2010). For

470 externally mixed aerosols, chemical species can be divided into two modes, LH and MH mode, based on their hygroscopic properties. In general, BC and organics (or only HOA) are classified into LH mode, whereas inorganics and/or OOA are classified into MH mode in externally mixed aerosols. In this study, we identify and quantify chemical species of each mode for externally mixed aerosols with GF distribution data and size-resolved chemical data to understand the relationship between the mixing

475 state and chemical composition of atmospheric aerosols. Figure 11 shows the scatterplot of the Peak 1 (LH mode) area ratio vs. the volume fraction of each chemical species for different diameters. As mentioned above, the area ratio of each mode in the GF distribution ($dN/dlog(GF)$) corresponds the number fraction of particles in each mode and thereby can be compared directly with the volume fraction of each chemical species for a diameter. Note that only the observed externally mixed aerosols

480 (Type 1) are used for comparison. The volume fraction of HOA is positively correlated with Peak 1 area ratio (Fig.10a) when all sizes are combined but not for each diameter. The slope between them and the coefficient of determination (R^2) were 0.73 and 0.58, respectively. In other words, the HOA volume fraction can explain about 58% of the variation of number fraction for LH mode in externally mixed aerosols. We can infer that the unexplained part can be complemented by BC, which is known to be

485 hydrophobic. Unfortunately, size-resolved BC is not available in this study. The results in Fig. 10b (LH mode vs. volume fraction of organics) and 10c (LH mode vs. volume fraction of OOA) also support this

speculation. The volume fraction of all organics, including both HOA and OOA (Fig. 10b), is much higher than the number fraction of LH mode. Furthermore, negative and even weak correlation was shown between the volume fraction of the OOA and Peak 1 area ratio (Fig. 10c).
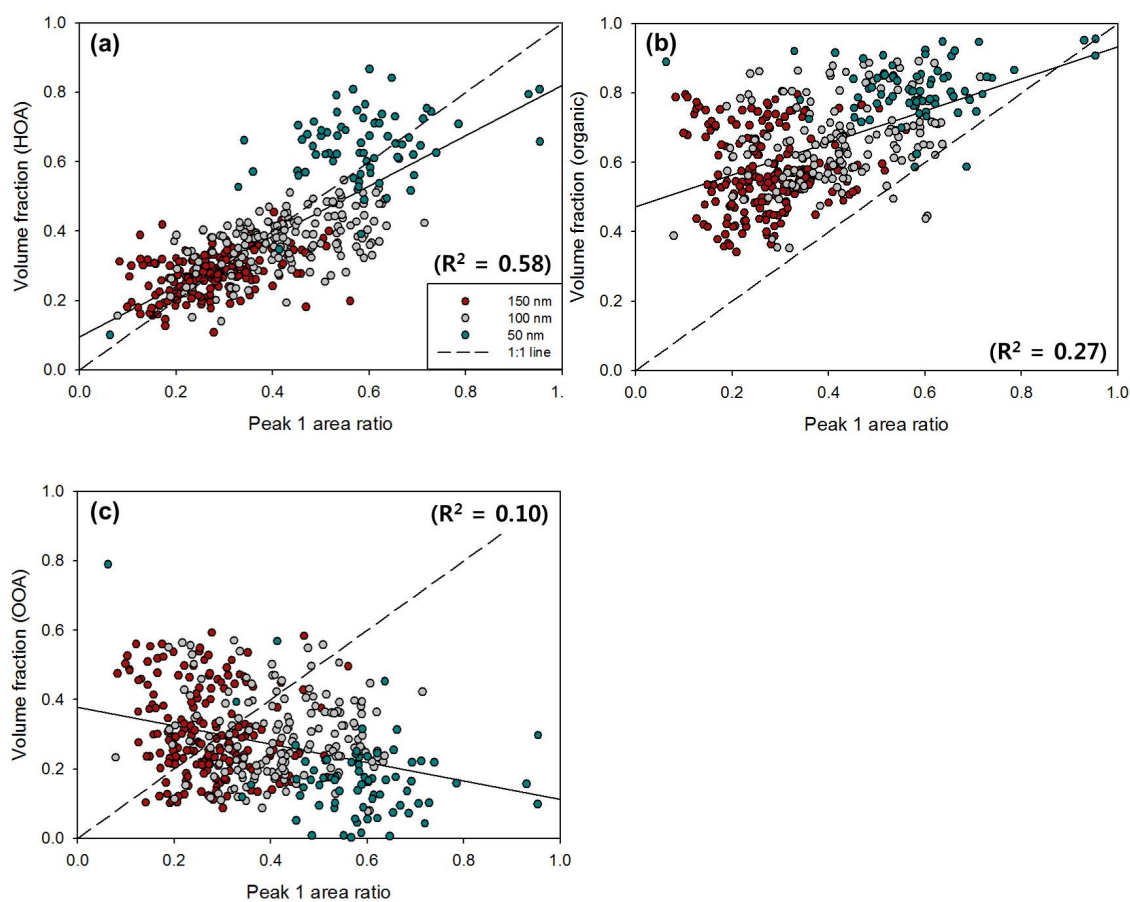
490

Figure 11. Scatterplots between Peak 1 (LH mode) area ratio and volume fraction of (a) HOA, **(b)** organics (HOA+OOA) and **(c)** OOA for 50 nm (turquoise), 100 nm (grey) and 150 nm (red) particles. Dashed line and solid line present 1:1 line and linear regression line, respectively. The coefficient of determination (R^2) of each scatterplot is indicated.

495
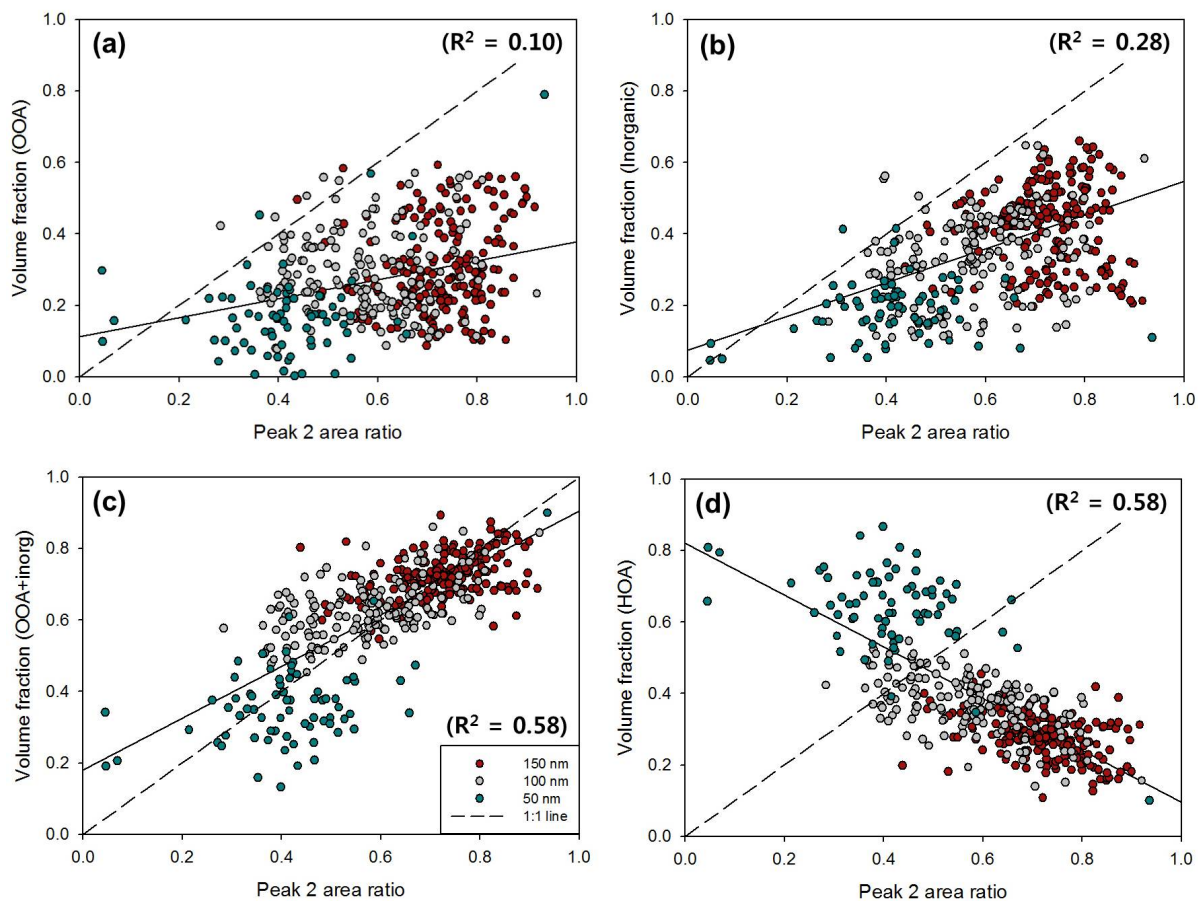
Figure 12. Scatterplots between Peak 2 (MH mode) area ratio and volume fraction of (a) **OOA,** (b) **inorganic,** (c) **OOA+inorganic, and** (d) **HOA for 50 nm (turquoise), 100 nm (grey) and 150 nm (red) particles. Dashed line and solid line present 1:1 line and linear regression line, respectively. The coefficient of determination (R^2) of each scatterplot is indicated.**

For Peak 2 (MH mode), OOA (Fig. 12a) and inorganic (Fig. 12b) did show a positive correlation with Peak 2 area ratio, but it was not strong enough to explain a significant portion of MH mode. The sum of OOA and inorganic volume fraction (Fig. 12c) can explain a significant portion of MH mode variation in externally mixed aerosols, whereas a negative correlation is clearly shown between the volume fraction of HOA and Peak 2 area ratio (Fig. 12d). For individual diameters, correlations tended to be stronger for larger (100 nm and 150 nm) than smaller (50 nm) diameters. It is related to the fact that there are high uncertainties of size-resolved chemical composition data for small diameters. Nevertheless, these results give meaningful implications that HTDMA – HR-ToF-AMS dataset could

510 successfully explain connections between aerosol composition and hygroscopic mode (i.e., mixing state) and their relative contributions. Specifically, the volume fraction of HOA (and BC) can explain a major portion of the number fraction of LH mode particles. For MH mode, volume fraction of the sum of OOA and inorganics, , can explain the number fraction of MH mode particles. During the campaign, externally mixed aerosols (Type 1) were observed about 50% of the total period, meaning that LH mode

515 particles (i.e., HOA) and MH mode particles (i.e., inorganics and OOA) were externally mixed in the atmosphere half of the time during the campaign.

5. Summary and Conclusions

This study investigated the chemical effects on size-resolved hygroscopicity of urban aerosols

520 based on the KORUS-AQ field campaign data. Mainly, the information of size-resolved hygroscopicity and mixing state of aerosols for four dry diameters (30, 50, 100 and, 150 nm) was obtained by HTDMA. During the campaign period, averaged mass concentration of PM_1 aerosols was 19.1 μg m^{-3}, and observed anions were fully neutralized by $NH_4{}^+$. On average, organics occupied more than 40% of the mass concentration for non-refractory aerosols. Among three organic factors (HOA, SV-OOA, and LV-

525 OOA) analyzed by PMF analysis, OOA accounted for 66.4%. Substantial differences of aerosol chemical composition were shown in the two specific periods, organic dominant period (Period A) and inorganic dominant period (Period B), and these differences affected aerosol hygroscopicity of each period. The averaged κ values ranged from 0.11 to 0.24, and as in other urban regions κ clearly showed size-dependency. Estimated κ values calculated with bulk chemical composition data and oxidation

530 parameters, f_{44} and O/C (κ_{chem}), showed good correspondence with measured κ values (κ_{HTDMA}) for 150 nm particles. It implies that chemical composition is closely associated with aerosol hygroscopicity, and such oxidation parameters are suitable for representing the hygroscopicity of organic aerosols. However, for small particles such good relationship was not shown between κ_{HTDMA} and κ_{chem} due

to the fact that bulk chemistry might have been determined mainly by larger particles that might not have the same chemical composition of small particles.

These results emphasize the importance of size-resolved chemical composition data for examining the relationship between chemical composition and aerosol hygroscopicity, especially for small particles. Furthermore, the size-resolved organic factor information is essential as organic particles are mostly small. The m/z tracer method is applied in this study to obtain size-resolved organic factors. m/z 57 and m/z 44 are used as AMS spectral markers for HOA and OOA, respectively. According to the campaign averaged size-resolved volume fraction, the volume fraction of inorganics, which is known to be hygroscopic, increases as particle size increases. For organics, a decrease of HOA and an increase of OOA are shown as particle size increases, which support the size-dependency of aerosol hygroscopicity. Particularly, the size-resolved organic factor can give a detailed explanation of the diurnal variation of κ for small particles. Low κ in the morning is associated with the large volume fraction of HOA, whereas high κ in the afternoon is related to the large volume fraction of OOA. Scatterplots of volume fraction of organic factors vs. κ values clearly illustrate that chemical composition is closely associated with hygroscopic properties of aerosols, not only for large particles but also for small particles.

Lastly, the characteristics of the mixing state of aerosols were investigated in association with size-resolved chemical composition data. Externally mixed aerosols were observed about 50% of the time during the campaign period, especially for large particles. Importantly, the number fraction and GF value of MH mode increased as particle size increased. The relationship between the number fraction of each hygroscopicity mode and volume fraction of different chemical composition is analyzed. For example, the HOA volume fraction explained about 60% of the variation of LH mode number fraction for externally mixed aerosols. It can be inferred that the volume fraction of BC can explain the rest. On the other hand, the chemical composition of MH mode can be explained by the sum of inorganics and OOA rather than the volume fraction of each of OOA and inorganics. Unlike previous studies that used

hygroscopicity of ensemble particles without mixing state information, such relationship of chemical

560 composition – mixing state – hygroscopicity of atmospheric particles can be of crucial use in accurate

N_{CCN} prediction.

It can be concluded that size-resolved chemical composition data did provide more detailed and essential information than bulk data, which are highly needed when examining the relationship between chemical composition and hygroscopic properties of aerosols as well as the mixing state.

565 Specified organic factors were found to be critically important, mainly in estimating the hygroscopicity of small particles as organics occupied a significant portion of these particles. Although the two OA factors, HOA and OOA, can represent the total organic mass concentration and can also explain the variability of κ reasonably well, more detailed analysis can be made when more spectral tracers are added to derive sub-divided organic factors. To note is that organic aerosols do not always behave

570 ideally and show an apparent discrepancy in hygroscopic growth between sub- and supersaturated conditions (Petters et al., 2009; Wex et al., 2009). If hygroscopic growth were measured under a supersaturated condition, the estimated hygroscopicity parameter would be significantly higher than those estimated in this study under sub-saturated condition, due to the contribution of enhanced hygroscopic growth of organic components of aerosols. This would surely affect the CCN prediction

575 results but it is uncertain how much that would be at this point. Perhaps, however, the overestimating tendency of $κ_{chem}$ shown in Fig. 4 may be reduced as the measured κ would become higher. The results presented here were obtained during the spring/summer season. It would be very informative to make the observation during other seasons to find seasonal variability, especially during the winter season, when aerosol properties and meteorological conditions would be so much different from spring/summer.

580 Our future work includes such an endeavor.

Data availability. KORUS-AQ data are available via https://espo.nasa.gov/korus-aq/content/KORUS-AQ (doi: 10.5067/Suborbital/KORUSAQ/DATA01).

585 *Author contribution.* NK carried out the observation, analyzed the data and wrote the manuscript. SSY acquired funding for the study, contributed to the analysis of the data and edited the manuscript. MP contributed to carrying out the observation and analyzing the data. JSP, HJS, JYA provided HR-ToF-AMS data. All authors discussed the results, read and commented on the manuscript.

590 *Competing interests.* The authors declare no competing interests.

Acknowledgment. This work was supported by the National Research Foundation of Korea (NRF) grant funded by the Korean government (MSIT) (No.NRF-2018R1A2B2006965).

595 **References**

Alfarra, M. R.; Coe, H.; Allan, J. D.; Bower, K. N.; Boudries, H.; Canagaratna, M. R.; Jimenez, J. L.; Jayne, J. T.; Garforth, A.; Li, S.-M.; Worsnop, D. R.: Characterization of urban and regional organic aerosols in the lower Fraser Valley using two Aerodyne AerosolMassSpectrometers. Atmos. Environ, 5745-5758, 2004.

Allan, J. D., J. L. Jimenez, P. I. Williams, M. R. Alfarra, K. N. Bower, J. T. Jayne, H. Coe, and D. R. Worsnop, Quantitative
600 sampling using an Aerodyne aerosol mass spectrometer, 1, Techniques of data interpretation and error analysis, J. Geophys. Res., 108(D3), 4090, doi:10.1029/2002JD002358, 2003.

Allan, J. D., Bower, K. N., Coe, H., Boudries, H., Jayne, J. T., Canagaratna, M. R., Millet, D. B., Goldstein, A. H., Quinn, P. K., Weber, R. J., and Worsnop, D. R.: Submicron aerosol composition at Trinidad Head, California, during ITCT 2K2: Its relationship with gas phase volatile organic carbon and assessment of instrument performance, J. Geophys. Res., 109(D23),
605 D23S24, doi:10.1029/2003JD004208, 2004.

Andreae, M.O., Rosenfeld, D.: Aerosol-cloud-precipitation interactions. Part 1. The nature and sources of cloud-active aerosol. Earth-Sci. Rev. 89, 13e41, 2008.

Baltensperger, U., Streit, N., Weingartner, E., Nyeki, S., Prévôt, A. S. H., Van Dingenen, R., Virkkula, A., Putaud, J. P., Even, A., Ten Brink, H., Blatter, A., Neftel, A. and Gäggeler, H. W.: Urban and rural aerosol characterization of summer smog
610 events during the PIPAPO field campaign in Milan, Italy, J. Geophys. Res. Atmos., 107(22), doi:10.1029/2001JD001292, 2002.

Berg, O. H., Swietlicki, E. and Krejci, R.: Hygroscopic growth of aerosol particles in the marine boundary layer over the Pacific and Southern Oceans during the First Aerosol Characterization Experiment (ACE 1), J. Geophys. Res., 103(D13), 16535–16545, doi:10.1029/97JD02851, 1998.

615 Bhattu, D., and S. N. Tripathi: CCNclosure study: Effects of aerosol chem-ical composition and mixing state,J.Geophys. Res. Atmos.,120, 766–783,doi:10.1002/2014JD021978, 2015.

Canagaratna, M. R.; Jayne, J. T.; Ghertner, D. A.; Herndon, S.; Shi, Q.; Jimenez, J. L.; Silva, P. J.; Williams, P.; Lanni, T.; Drewnick, F.; Demerjian, K. L.; Kolb, C. E.; Worsnop, D. R.: Chase studies of particulate emissions from in-use New York city vehicles. Aerosol Sci. Technol., 38, 555-573, 510.1080/ 02786820490465504, 2004.

620 Chang, R. Y.-W., Slowik, J. G., Shantz, N. C., Vlasenko, A., Liggio, J., Sjostedt, S. J., Leaitch, W. R., and Abbatt, J. P. D.: The hygroscopicity parameter _ of ambient organic aerosol at a field site subject to biogenic and anthropogenic influences: relationship to degree of aerosol oxidation, Atmos. Chem. Phys., 10, 5047–5064, doi:10.5194/acp-10-5047-2010, 2010.

Cerully, K. M., Bougiatioti, A., Hite Jr., J. R., Guo, H., Xu, L., Ng, N. L., Weber, R., and Nenes, A.: On the link between hygroscopicity, volatility, and oxidation state of ambient and water-soluble aerosols in the southeastern United States, Atmos.
625 Chem. Phys., 15, 8679–8694, https://doi.org/10.5194/acp15-8679-2015, 2015

Cheng, Y. F., Wiedensohler, A., Eichler, H., Heintzenberg, J., Tesche, M., Ansmann, A., Wendisch, M., Su, H., Althausen, D., and Herrmann, H.: Relative humidity dependence of aerosol optical properties and direct radiative forcing in the surface boundary layer at Xinken in Pearl River Delta of China: An observation based numerical study, Atmos. Environ., 42, 6373–6397, https://doi.org/10.1016/j.atmosenv.2008.04.009, 2008

630 Cocker, D. R., Whitlock, N. E., Flagan, R. C. and Seinfeld, J. H.: Hygroscopic properties of pasadena, california aerosol, Aerosol Sci. Technol., 35(2), 637–647, doi:10.1080/02786820120653, 2001.

Cross, E. S., J. G. Slowik, P. Davidovits, J. D. Allan, D. R. Worsnop, J. T. Jayne, D. K. Lewis, M. Canagaratna, and T. B. Onasch: Laboratory and ambient particle density determinations using light scattering in conjunction with aerosol mass spectrometry, *Aerosol Sci. Technol.*, **41**, 343– 359, 2007.

635 Peter F. DeCarlo , Jay G. Slowik , Douglas R. Worsnop , Paul Davidovits & Jose L. Jimenez: Particle Morphology and Density Characterization by Combined Mobility and Aerodynamic Diameter Measurements. Part 1: Theory, Aerosol Science and Technology, 38:12, 1185-1205, DOI: 10.1080/027868290903907, 2004.

Deng, Y., Yai, H., Fujinari, H., Kawana, K., Nakayama, T., and Mochida, M.: Diurnal variation and size dependence of the hygroscopicity of organic aerosol at a forest site in Wakayama, Japan: their relationship to CCN concentrations, Atmos.
640 Chem. Phys., 19, 5889–5903, https://doi.org/10.5194/acp-19-5889-2019, 2019.

Enroth, J., Mikkilä, J., Németh, Z., Kulmala, M., and Salma, I.: Wintertime hygroscopicity and volatility of ambient urban aerosol particles, Atmos. Chem. Phys., 18, 4533–4548, https://doi.org/10.5194/acp-18-4533-2018, 2018.

Ervens, B., Cubison, M. J., Andrews, E., Feingold, G., Ogren, J. A., Jimenez, J. L., Quinn, P. K., Bates, T. S., Wang, J., Zhang, Q., Coe, H., Flynn, M. and Allan, J. D.: CCN predictions using simplified assumptions of organic aerosol composition and
645 mixing state: A synthesis from six different locations, Atmos. Chem. Phys., 10(10), 4795–4807, doi:10.5194/acp-10-4795-2010, 2010.

Florou, K., Papanastasiou, D. K., Pikridas, M., Kaltsonoudis, C., Louvaris, E., Gkatzelis, G. I., Patoulias, D., Mihalopoulos, N., and Pandis, S. N.: The contribution of wood burning and other pollution sources to wintertime organic aerosol levels in two Greek cities, Atmos. Chem. Phys., 17, 3145–3163, https://doi.org/10.5194/acp-17-3145-2017, 2017.

650 Gunthe, S. S., King, S. M., Rose, D., Chen, Q., Roldin, P., Farmer, D. K., Jimenez, J. L., Artaxo, P., Andreae, M. O., Martin, S. T., and P̈oschl, U.: Cloud condensation nuclei in pristine tropical rainforest air of Amazonia: size-resolved measurements and modeling of atmospheric aerosol composition and CCN activity, Atmos. Chem. Phys., 9, 7551–7575, http://www.atmos-chem-phys.net/9/7551/2009/, 2009.

Gysel, M., Crosier, J., Topping, D. O., Whitehead, J. D., Bower, K. N., Cubison, M. J., Williams, P. I., Flynn, M. J., McFiggans,
655 G. B., Coe, H.: Closure study between chemical composition and hygroscopic growth of aerosol particles during TORCH2. Atmospheric Chemistry and Physics 7, 6131-6144, 2007.

Heo, J.-B., Hopke, P. K., and Yi, S.-M.: Source apportionment of PM$_{2.5}$ in Seoul, Korea, Atmos. Chem. Phys., 9, 4957–4971, https://doi.org/10.5194/acp-9-4957-2009, 2009.

Hong, J., Xu, H., Tan, H., Yin, C., Hao, L., Li, F., Cai, M., Deng, X., Wang, N., Su, H., Cheng, Y., Wang, L., Petäjä, T., and
660 Kerminen, V.-M.: Mixing state and particle hygroscopicity of organic-dominated aerosols over the Pearl River Delta region in China, Atmos. Chem. Phys., 18, 14079–14094, https://doi.org/10.5194/acp-18-14079-2018, 2018.

Hong, J., Kim, J., Nieminen, T., Duplissy, J., Ehn, M., Äijälä, M., Hao, L. Q., Nie, W., Sarnela, N., Prisle, N. L., Kulmala, M., Virtanen, A., Petäjä, T., and Kerminen, V.-M.: Relating the hygroscopic properties of submicron aerosol to both gas- and particle-phase chemical composition in a boreal forest environment, Atmos. Chem. Phys., 15, 11999–12009,
665 https://doi.org/10.5194/acp-15-11999-2015, 2015.

IPCC: Climate Change: the physical science basis, Working Group I Contribution to the Fifth Assessment Report of the Intergovernmental Panel on Climate Change, Cambridge University Press, Cambridge, UK, New York, NY, USA 2013, 2013.

Jiang, R. X., Tan, H. B., Tang, L. L., Cai, M. F., Yin, Y., Li, F., Liu, L., Xu, H. B., Chan, P. W., Deng, X. J., and Wu, D.: Comparison of aerosol hygroscopicity and mixing state between winter and summer seasons in Pearl River Delta region, China, Atmos. Res., 169, 160–170, 2016.

670

Jurányi, Z., Tritscher, T., Gysel, M., Laborde, M., Gomes, L., Roberts, G., Baltensperger, U., and Weingartner, E.: Hygroscopic mixing state of urban aerosol derived from size-resolved cloud condensation nuclei measurements during the MEGAPOLI campaign in Paris, Atmos. Chem. Phys., 13, 6431-6446, https://doi.org/10.5194/acp-13-6431-2013, 2013.

Kim, J. H., Yum, S. S., Shim, S., Yoon, S.-C., Hudson, J. G., Park, J., and Lee, S.-J.: On aerosol hygroscopicity, cloud condensation nuclei (CCN) spectra and critical supersaturation measured at two remote islands of Korea between 2006 and 2009, Atmos. Chem. Phys., 11, 12627–12645, https://doi.org/10.5194/acp-11-12627-2011, 2011.

675

Kim, N., Park, M., Yum, S. S., Park, J. S., Song, I. H., Shin, H. J., Ahn, J. Y., Kwak, K.-H., Kim, H., Bae, G.-N. and Lee, G.: Hygroscopic properties of urban aerosols and their cloud condensation nuclei activities measured in Seoul during the MAPS-Seoul campaign, Atmos. Environ., 153, 217–232, doi:10.1016/j.atmosenv.2017.01.034, 2017.

680 Kim, N., Park, M., Yum, S. S., Park, J. S., Shin, H. J., Ahn, J. Y.: Impact of urban aerosol properties on cloud condensation nuclei (CCN) activity during the KORUS-AQ field campaign, Atmos Environ., 185, 221-236, https://doi.org/10.1016/j.atmosenv.2018.05.019, 2018a.

Kim, H., Zhang, Q., and Heo, J.: Influence of intense secondary aerosol formation and long-range transport on aerosol chemistry and properties in the Seoul Metropolitan Area during spring time: results from KORUS-AQ, Atmos. Chem. Phys., 18, 7149–7168, https://doi.org/10.5194/acp-18-7149-2018, 2018b.

685

Kim, S.-W., Choi, I.-J., and Yoon, S.-C.: A multi-year analysis of clear-sky aerosol optical properties and direct radiative forcing at Gosan, Korea (2001–2008), Atmos. Res., 95, 279–287, 2010.

Kuwata, M., Zorn, S. R., and Martin, S. T.: Using Elemental Ratios to Predict the Density of Organic Material Composed of Carbon, Hydrogen, and Oxygen, Environ. Sci. Technol., 46, 787– 794, https://doi.org/10.1021/es202525q, 2012.

690 Larkin A, van Donkelaar A, Geddes JA, Martin RV, Hystad P. Relationships between changes in urban characteristics and air quality in East Asia from 2000 to 2010. Environ Sci Technol, 50(17), 9142–9. https://doi.org/10.1021/acs.est.6b02549.2016

Levin, E.J.T., Prenni, A.J., Petters, M.D., Kreidenweis, S.M., Sullivan, R.C., Atwood, S.A.,Ortega, J., DeMott, P.J., Smith, J.N.: An annual cycle of size-resolved aerosol hygroscopicity at a forested site in Colorado. J. Geophys. Res. 117, D06201, 2012.

695 Levin, E.J.T., Prenni, A.J., Palm, B.B., Day, D.A., Campuzano-Jost, P., Winkler, P.M., Kreidenweis, S.M., DeMott, P.J., Jimenez, J.L., Smith, J.N.: Size-resolved aerosol composition and its link to hygroscopicity at a forested site in Colorado. Atmos. Chem. Phys. 14, 2657e2667. http://dx.doi.org/10.5194/acp-14-2657- 2014, 2014.

Liu, B. Y. H., Pui, D. Y. H., Whitby, K. T., Kittelson, D. B. and Kousaka, Y., and McKenzie, R. L.: The aerosol mobility chromatograph: A new detector for sulfuric acid aerosols, Atmos. Environ., 12(1–3), 99–104, doi:10.1016/0004-6981(78)90192-0, 1978.

700

Liu, X., Gu, J., Li, Y., Cheng, Y., Qu, Y., Han, T., Wang, J., Tian, H., Chen, J., and Zhang, Y.: Increase of aerosol scattering by hygroscopic growth: Observation, modeling, and implications on visibility, Atmos. Res., 132–133, 91–101, https://doi.org/10.1016/j.atmosres.2013.04.007, 2013.

Massling, A., Stock, M. and Wiedensohler, A.: Diurnal, weekly, and seasonal variation of hygroscopic properties of submicrometer urban aerosol particles, Atmos. Environ., 39(21), 3911–3922, doi:10.1016/j.atmosenv.2005.03.020, 2005.

Massling, A., Leinert, S., Wiedensohler, A. and Covert, D.: Hygroscopic growth of sub-micrometer and one-micrometer aerosol particles measured during ACE-Asia, Atmos. Chem. Phys. Discuss., 6(6), 12267–12300, doi:10.5194/acpd-6-12267-2006, 2006.

Maßling, A., Wiedensohler, A., Busch, B., Neusüß, C., Quinn, P., Bates, T. and Covert, D.: Hygroscopic properties of different aerosol types over the Atlantic and Indian Oceans, Atmos. Chem. Phys., 3(5), 1377–1397, doi:10.5194/acp-3-1377-2003, 2003.

McFiggans, G., Artaxo, P., Baltensperger, U., Coe, H., Facchini, M. C., Feingold, G., Fuzzi, S., Gysel, M., Laaksonen, A., Lohmann, U., Mentel, T. F., Murphy, D. M., O'Dowd, C. D., Snider, J. R. and Weingartner, E.: The effect of physical and chemical aerosol properties on warm cloud droplet activation, Atmos. Chem. Phys., 2593–2649, doi:10.5194/acpd-5-8507-2005, 2006.

Meng, J. W., Yeung, M. C., Li, Y. J., Lee, B. Y. L., and Chan, C. K.: Size-resolved cloud condensation nuclei (CCN) activity and closure analysis at the HKUST Supersite in Hong Kong, Atmos. Chem. Phys., 14, 10267–10282, https://doi.org/10.5194/acp-14-10267-2014, 2014.

Mei, F., Setyan, A., Zhang, Q., and Wang, J.: CCN activity of organic aerosols observed downwind of urban emissions during CARES, Atmos. Chem. Phys., 13, 12155–12169, https://doi.org/10.5194/acp-13-12155-2013, 2013.

Moore, R. H., Nenes, A. and Medina, J.: Scanning mobility CCN analysis-A method for fast measurements of size-resolved CCN distributions and activation kinetics, Aerosol Sci. Technol., 44(10), 861–871, doi:10.1080/02786826.2010.498715, 2010.

O'Haver, T. C.: Pragmatic introduction to signal processing 2016: Applications in scientific measurement. Independently published, 2016.

Paatero, P. and Hopke, P. K.: Discarding or downweighting high-noise variables in factor analytic models, Anal.Chim.Acta, 490 (1-2),277-89, 2003.

Paramonov, M., Aalto, P. P., Asmi, A., Prisle, N., Kerminen, V.-M., Kulmala, M., and Petäjä, T.: The analysis of size-segregated cloud condensation nuclei counter (CCNC) data and its implications for cloud droplet activation, Atmos. Chem. Phys., 13, 10285-10301, https://doi.org/10.5194/acp-13-10285-2013, 2013.

Petters, M. D. and Kreidenweis, S. M.: A single parameter representation of hygroscopic growth and cloud condensation nucleus activity, Atmos. Chem. Phys., 7, 1961–1971, doi:10.5194/acp-7- 1961-2007, 2007.

Petters, M. D., Wex, H., Carrico, C. M., Hallbauer, E., Massling, A., McMeeking, G. R., Poulain, L., Wu, Z., Kreidenweis, S. M., and Stratmann, F.: Towards closing the gap between hygroscopic growth and activation for secondary organic aerosol – Part 2: Theoretical approaches, Atmos. Chem. Phys., 9, 3999–4009, https://doi.org/10.5194/acp-9-3999-2009, 2009.

Reilly, P. J. and Wood, R. H.: Prediction of Properties of Mixed Electrolytes from Measurements on Common Ion Mixtures, J. Phys. Chem., 73 (12), 4292-4297, 1969.

Ren, J., Zhang, F., Wang, Y., Collins, D., Fan, X., Jin, X., Xu, W., Sun, Y., Cribb, M., and Li, Z.: Using different assumptions of aerosol mixing state and chemical composition to predict CCN concentrations based on field measurements in urban Beijing, Atmos. Chem. Phys., 18, 6907–6921, https://doi.org/10.5194/acp-18-6907-2018, 2018.

Rissler, J., Swietlicki, E., Zhou, J., Roberts, G., Andreae, M. O., Gatti, L. V., and Artaxo, P.: Physical properties of the sub-micrometer aerosol over the Amazon rain forest during the wet- to-dry season transition – comparison ofmodeled and measured CCN concentrations, Atmos. Chem. Phys., 4, 2119–2143, 2004, http://www.atmos-chem-phys.net/4/2119/2004/, 2004.

Rogers, R. R. and Yau, M. K.: A short course in cloud physics, vol. 113, International Series in Natural Philosophy, Butterworth- Heinemann, third edn, 1989.

Rosenfeld, D., Sherwood, S., Wood, R., and Donner, L.: Climate effects of aerosol-cloud interactions, science, 343, 379–380, https://doi.org/10.1126/science.1247490, 2014.

Stokes, R. H. and Robinson, R. A.: Interactions in aqueous nonelectrolyte solutions. I. Solute-solvent equilibria, J. Phys. Chem., 70, 2126–2130, 1966.

Su, H., Rose, D., Cheng, Y. F., Gunthe, S. S., Massling, A., Stock, M., Wiedensohler, A., Andreae, M. O., and Pöschl, U.: Hygroscopicity distribution concept for measurement data analysis and modeling of aerosol particle mixing state with regard to hygroscopic growth and CCN activation, Atmos. Chem. Phys., 10, 7489–7503, https://doi.org/10.5194/acp-10-7489-2010, 2010.

Swietlicki, E., Zhou, J. C., Covert, D. S., Hameri, K., Busch, B. and co-authors: Hygroscopic properties of aerosol particles in the northeastern Atlantic during ACE-2. Tellus 52B, 201–227, 2000.

Swietlicki, E., Hansson, H. C., Hämeri, K., Svenningsson, B., Massling, A., Mcfiggans, G., Mcmurry, P. H., Petäjä, T., Tunved, P., Gysel, M., Topping, D., Weingartner, E., Baltensperger, U., Rissler, J., Wiedensohler, A. and Kulmala, M.: Hygroscopic properties of submicrometer atmospheric aerosol particles measured with H-TDMA instruments in various environments - A review, Tellus, Ser. B Chem. Phys. Meteorol., 60 B(3), 432–469, doi:10.1111/j.1600-0889.2008.00350.x, 2008.

Tang, I. N.: Chemical and size effects of hygroscopic aerosols on light scattering coefficients, J. Geophys. Res.-Atmos., 101, 19245–19250, https://doi.org/10.1029/96JD03003, 1996.

Thalman, R., Sá, S.S. de, Palm, B.B., Barbosa, H.M.J., Pöhlker, M.L., Alexander, M.L., Brito, J., Carbone, S., Castillo, P., Day, D.A.: CCN activity and organic hygroscopicity of aerosols downwind of an urban region in central Amazonia: seasonal and diel variations and impact of anthropogenic emissions. Atmos. Chem. Phys. 17, 11779–11801, 2017.

Topping, D. O., McFiggans, G. B., and Coe, H.: A curved multi-component aerosol hygroscopicity model framework: Part 2 – Including organic compounds, Atmos. Chem. Phys., 5, 1223–1242, https://doi.org/10.5194/acp-5-1223-2005, 2005.

Tomlinson, J. M., Li, R. J. and Collins, D. R.: Physical and chemical properties of the aerosol within the southeastern Pa- cific marine boundary layer. J. Geophys. Res.-Atmos. 112, D12211, doi:12210.11029/12006JD007771, 2007.

Ulbrich, I. M., Canagaratna, M. R., Zhang, Q., Worsnop, D. R., and Jimenez, J. L.: Interpretation of organic components from

Positive Matrix Factorization of aerosol mass spectrometric data, Atmos. Chem. Phys., 9, 2891–2918, https://doi.org/10.5194/acp-9-2891-2009, 2009.

Wang, J., Cubison, M. J., Aiken, A. C., Jimenez, J. L. and Collins, D. R.: The importance of aerosol mixing state and size-resolved composition on CCN concentration and the variation of the importance with atmospheric aging of aerosols, Atmos. Chem. Phys., 10(15), 7267–7283, doi:10.5194/acp-10-7267-2010, 2010.

Wang, Y., Wu, Z., Ma, N., Wu, Y., Zeng, L., Zhao, C., & Wiedensohler, A.: Statistical analysis and parameterization of the hygroscopic growth of the sub-micrometer urban background aerosol in Beijing. Atmospheric Environment, 175, 184– 191, 2018.

Wang, Y., Zhang, F., Li, Z., Tan, H., Xu, H., Ren, J., Zhao, J., Du, W., Sun, Y.: Enhanced hydrophobicity and volatility of submicron aerosols under severe emission control conditions in Beijing. Atmos. Chem. Phys. 17, 5239–5251. http://dx.doi.org/ 10.5194/acp-17-5239-2017, 2017.

Wex, H., Petters, M. D., Carrico, C. M., Hallbauer, E., Massling, A., McMeeking, G. R., Poulain, L., Wu, Z., Kreidenweis, S. M., and Stratmann, F.: Towards closing the gap between hygroscopic growth and activation for secondary organic aerosol: Part 1 – Evidence from measurements, Atmos. Chem. Phys., 9, 3987–3997, https://doi.org/10.5194/acp-9-3987-2009, 2009.

Wu, Z. J., Zheng, J., Shang, D. J., Du, Z. F., Wu, Y. S., Zeng, L. M., Wiedensohler, A., and Hu, M.: Particle hygroscopicity and its link to chemical composition in the urban atmosphere of Beijing, China, during summertime, Atmos. Chem. Phys, 16, 1123-1138, doi: 10.5194/acp-16-1123-2016, 2016.

Wu, Z. J., Poulain, L., Henning, S., Dieckmann, K., Birmili, W., Merkel, M., van Pinxteren, D., Spindler, G., Müller, K., Stratmann, F., Herrmann, H., and Wiedensohler, A.: Relating particle hygroscopicity and CCN activity to chemical composition during the HCCT-2010 field campaign, Atmos. Chem. Phys., 13, 7983–7996, doi:10.5194/acp-13-7983-2013, 2013.

Ye, X., Tang, C., Yin, Z., Chen, J., Ma, Z., Kong, L., Yang, X., Wei, G., Geng, F.: Hygroscopic growth of urban aerosol particles during the 2009 Mirage- Shanghai Campaign. Atmos. Envion 64, 263e269, 2013.

Zdanovskii, A.: New methods for calculating solubilities of electrolytes in multicomponent systems, Zhur. Fiz. Khim., 22, 1475– 1485, 1948.

Zhang, Q., Alfarra, M. R., Worsnop, D. R., Allan, J. D., Coe, H., Canagaratna, M. R., and Jimenez, J. L.: Deconvolution and quantification of hydrocarbon-like and oxygenated organic aerosols based on aerosol mass spectrometry, Environ. Sci. Technol., 39, 4938–4952, 2005.

Zhang, R., Khalizov, A. F., Pagels, J., Zhang, D., Xue, H., and McMurry, P. H.: Variability in morphology, hygroscopicity, and optical properties of soot aerosols during atmospheric processing, P. Natl. Acad. Sci. USA, 105, 10291–10296, https://doi.org/10.1073/pnas.0804860105, 2008.

Zhang, Q., Jimenez, J. L., Canagaratna, M. R., Allan, J. D., Coe, H., Ulbrich, I., Alfarra, M. R., Takami, A., Middlebrook, A. M., Sun, Y. L., Dzepina, K., Dunlea, E., Docherty, K., DeCarlo, P. F., Salcedo, D., Onasch, T., Jayne, J. T., Miyoshi, T., Shimono, A., Hatakeyama, S., Takegawa, N., Kondo, Y., Schneider, J., Drewnick, F., Borrmann, S., Weimer, S., Demerjian, K., Williams, P., Bower, K., Bahreini, R., Cottrell, L., Griffin, R. J., Rautiainen, J., Sun, J. Y., Zhang, Y. M. and Worsnop, D. R.: Ubiquity and dominance of oxygenated species in organic aerosols in anthropogenically-influenced Northern

Hemisphere midlatitudes, Geophys. Res. Lett., 34(13), doi:10.1029/2007GL029979, 2007.

Zheng, G. J., Duan, F. K., Su, H., Ma, Y. L., Cheng, Y., Zheng, B., Zhang, Q., Huang, T., Kimoto, T., Chang, D., Pöschl, U., Cheng, Y. F., and He, K. B.: Exploring the severe winter haze in Beijing: the impact of synoptic weather, regional transport and heterogeneous reactions, Atmos. Chem. Phys., 15, 2969–2983, https://doi.org/10.5194/acp-15-2969-2015, 2015.

Zhou, J., Swietlicki, E., Berg, O. H., Aalto, P. P., Hämeri, K., Nilsson, E. D. and Leck, C.: Hygroscopic properties of aerosol particles over the central Arctic Ocean during summer, J. Geophys. Res. Atmos., 106(D23), 32111–32123, doi:10.1029/2000JD900426, 2001.

Zhou, J., Swietlicki, E., Hansson, H.C., Artaxo, P.: Submicrometer aerosol particle size distribution and hygroscopic growth measured in the Amazon rain forest during the wet season, J. Geophys. Res.-Atmos 107, 2002.